GBT MEMO 230

Working Notes On The Green Bank Telescope Laser Metrology System

David H. Parker

April 29, 2004

Contents

List of Figures

Abstract

This ongoing collection of notes, calculations, procedures, and references is intended to be an internal reference source for the GBT Antenna Metrology group as the instrumentation, architecture, and control systems are developed[1, 2]. Due to the large number of people that have contributed to the project; on a part-time basis, as consultants, as transient students, retired, or moved on to other things; and the fact that most areas remain to be firmly finalized, there is a significant problem with the formal documentation of all aspects of the project. It is hoped that this series of notes will serve as a basis for more formal documents as various aspects of the project come to completion, and as a pointer to various references that have influenced the design of the GBT Laser Metrology System.

This is the first major update since 1996, and is still woefully incomplete. With the suspension of work on the project, interest on the GBT specific metrology work has waned, so work has concentrated on writing stand-alone articles for publication. This report points to those articles and expands on the references in the archive documentation, so one at least has some orientation on where to start looking for more details. Hopefully it will be of some use. If you have any questions, I can be contacted at dhiramparker@ieee.org, and will be happy to try to point to the answer.

Chapter 1

Group Refractive Index

1.1 Introduction

One of the fundamental limitations for outdoor Electronic Distance Measurement (EDM) is the group refractive index of air [3, 4, 5, 6, 7, 8, 9, 10, 11, 12, 13, 14, 15, 16, 17, 18, 19, 20, 21, 22, 23, 24, 25].

1.2 Phase and Group Velocities

It is well known that, due to dispersion, the velocity of the envelope of a modulated signal is not the same as the velocity of the carrier signal. This can be qualitatively explained by a simple example. For a 780 nm laser (384 615.3GHz) amplitude modulated at 1.5 GHz, sidebands are generated at 384 616.8 GHz and 384 613.8 GHz. In a dispersive medium, the two sidebands propogate at slightly different speeds, and thus there is a phase shift between the two sidebands in the Fourier domain. Recall that this is the same as a phase shift of the modulating signal[26] in the time domain. Thus, the phase of the modulated signal is retarded in a dispersive medium.

This introduces a subtle problem using refractive optics to focus a modulated beam on a detector. From Huygens principle, a lens focuses a plane wave at the focal length of the lens, i.e., the propogation time is the same for all rays. However, due to the group refractive index, there is spherical aberation introduced for the modulated wave, i.e., the modulation phase of the beam through the center of the lens is not the same as the modulation phase of a beam that passes through an outer edge of the lens. This will be talke about more in the chapter on optics.

The index of refraction n is the ratio of the velocity in vacuum to the velocity in the medium at a single wavelength λ. The *group* index of refraction is the ratio of the velocity in vacuum to the velocity in the medium of the envelope (the information) of a modulated signal on a carrier of wavelength λ. For a dispersive medium, the group refractive index is

$$n_g = n - \frac{d\,n}{d\,\lambda}\lambda. \tag{1.1}$$

For convenience, the term group refractivity N_g[24] is used where

$$N_g = (n_g - 1) \times 10^6. \tag{1.2}$$

1.3 Atmospheric Changes in n_g

A detailed treatment of the group refractive index for air as a function of wavelength, temperature, pressure, and humidity is given in reference [24]. For laser Electronic Distance Measurement, it turns out that corrections for changes in temperature, humidity, and pressure are the limiting constraints

on the instrument. This was recognized from the outset of the GBT project [3] and has been a major point of research to find techniques to correct for the group index of refraction for outdoor measurements.

At the present time, two methods are actively being investigated. The first method involves calculating n_g from measurements of temperature, humidity, and pressure. The equations are good to about two parts in 10^8, so the limitations are the homogeneity of the atmosphere and the resolution of the weather instruments.

The second method is a direct reading of n_g using the laser as a refractometer over a long path length. This method is limited by the long term stability of the monuments and the homogeneity of the atmosphere.

Preliminary data from a simple weather station located near the panel experiment indicates the feasibility of the calculated method. The calculated and refractometer values for N_g differ by a few parts per million at times, but the calibration of the weather instruments is questionable. Calibrated weather instruments will be installed on two 45 meter towers around the GBT. Experiments will be conducted as soon as the first instruments are available to compare the calculated and refractometer methods.

A preliminary investigation has been completed on the application of acoustic thermometry. This method has the advantage of an integrated measurement over the path of interest (including paths on the telescope) without stringent stability requirements, but corrections for wind will require an array of detectors. Software and hardware has been successfully developed and tested to measure the propagation time of an audio pulse, using an autocorrelation technique.

1.3.1 Mathematica Program

Figure 1.1 is a Mathematica program that is used to calculate meteorological properties of air, and N_g for air and glass.

1.4 Meteorological Properties of Air

The saturation water vapor pressure for liquid water is calculated from equation (5.27) of reference [24],

$$\acute{E}_W = 6.112\,1(1.000\,7 + 3.46 \times 10^{-6} p) \exp\left[\frac{17.502\acute{t}}{240.97 + \acute{t}}\right]. \tag{1.3}$$

The saturation water vapor pressure for ice is calculated from equation (5.28) as

$$\acute{E}_{\text{ice}} = 6.111\,5(1.000\,3 + 4.18 \times 10^{-6} p) \exp\left[\frac{22.452\acute{t}}{272.55 + \acute{t}}\right], \tag{1.4}$$

where

$\acute{E}_W$ = saturation vapor pressure of liquid water (mb)
$\acute{E}_{\text{ice}}$ = saturation vapor pressure of ice (mb)
p = atmospheric pressure (mb)
$\acute{t}$ = dry bulb temperature (for relative humidity calculation) (°C).

The partial water vapor pressure, P_w, is calculated from the relative humidity, h, using equation (5.29)

$$P_w = \frac{\acute{E}_W h}{100}. \tag{1.5}$$

Reference [24] also gives the equations for calculating the partial water vapor pressure as a function of wet and dry bulb temperatures.

1.4.1 Dew Point

When the temperature drops to the point that the water vapor pressure is equal to the saturation water vapor pressure, dew will form on the retroreflectors and reflected power will fall. The dew point temperature, T_d, can be predicted as a function of total pressure and water vapor pressure from equation 1.3 by solving for t with

$$P_w = \acute{E}_W. \tag{1.6}$$

$$T_d = \frac{240.97\{\ln(P_w) - \ln[6.112\,1(1.000\,7 + 3.46 \times 10^{-6}p)]\}}{17.502 + \ln[6.112\,1(1.000\,7 + 3.46 \times 10^{-6}p)] - \ln(P_w)}. \tag{1.7}$$

1.4.2 Pressure Calibration

The pressure transducer must be calibrated against a mercury barometer. Corrections must be made for temperature and local gravity[7, 27, 28, 8]. The temperature correction for mercury is

$$p_t = p_r \left(\frac{1 + 0.000\,018\,4\,t}{1 + 0.000\,181\,8\,t}\right). \tag{1.8}$$

Gravity must be corrected for latitude and elevation. The latitude correction is

$$g_\phi = 980.616[1 - 0.002\,637\,3\cos(2\phi) + 0.000\,005\,9\cos^2(2\phi)]. \tag{1.9}$$

From Table 167 of reference [7], The elevation correction is

$$\begin{aligned} \Delta g_\phi \;=\; & -(3.085\,462 \times 10^{-4} + 2.27 \times 10^{-7}\cos(2\phi))Z \\ & +(7.254 \times 10^{-11} + 1.0 \times 10^{-13}\cos(2\phi))Z^2 \\ & -(1.517 \times 10^{-17} + 6 \times 10^{-20}\cos(2\phi))Z^3 \end{aligned} \tag{1.10}$$

where

$$\begin{aligned} g_\phi &= \text{sea} - \text{level acceleration of gravity (cm sec}^{-2}) && (1.11)\\ \Delta g_\phi &= \text{elevation correction} \\ Z &= \text{elevation (meters)} \\ p_l &= \text{local station pressure} \\ p_r &= \text{uncorrected barometer reading} \\ p_t &= \text{temperature corrected barometer reading} \\ t &= \text{temperature (°C)} \\ \phi &= \text{latitude.} && (1.12) \end{aligned}$$

The local station pressure is

$$p_l = \frac{p_t g}{980.665} \tag{1.13}$$

where

$$g = g_\phi + \Delta g_\phi. \tag{1.14}$$

The latitude in Green Bank is 38° 27'. The sea level gravity correction reduces to

$$g_\phi = 980.030(\text{cm sec}^{-2}). \tag{1.15}$$

The laser calibration lab barometer is located at elevation 797.3 meters above sea level. For this elevation, the correction is

$$\begin{aligned} \Delta g_\phi &= -.246 && (1.16)\\ g &= 979.784. && (1.17) \end{aligned}$$

The total correction is,

$$p_l = 0.999\,102\,p_t \tag{1.18}$$

$$= 0.999\,102\,p_r\left(\frac{1+0.000\,018\,4\,t}{1+0.000\,181\,8\,t}\right). \tag{1.19}$$

The reading must then be converted from mm Hg to mb where

$$1.333\,224 \text{ mb/mm Hg.} \tag{1.20}$$

For example, an uncorrected measurement of 700 mm Hg at 20 °C would be

$$p_r = 700 \text{ mm Hg} \tag{1.21}$$

$$p_l = 697.09 \text{ mm Hg}$$

$$= 929.37 \text{ mb.} \tag{1.22}$$

For the GBT, elevation is also a significant correction. At 20 °C, the pressure changes about .11 mb/m, or about 16 mb from ground to the highest point. See Tables 57-62 of reference [7] for the exact pressure correction. The interferometer weather station pressure transducer is at elevation 803.8 m, the GBT top of track is at elevation 807.4 m.

Gravity Stations

After some investigation, it turns out that there are three NOAA/NGS gravity stations at NRAO[29]. Brass marker NGS stations were established and absolute gravity measurements were made in 1988. Station designated "Green Bank AA" is located in the basement of the interferometer building. Station "Green Bank B" is located at the base of the antenna next to the interferometer building, and station "Green Bank AB" is in the 40' telescope control room. Published values are
Green Bank AA at 2622 feet = 979.795 654 gal ±5 microgal
Green Bank B at 2642 feet = 979.794 688gal
Green Bank AB at 2693 feet= 979.792 146gal, Where gal = 0.01m/s^2.

1.5 Calculated n_g for Air

From Appendix A of reference [24], the density factor for dry air, D_s, is

$$D_s = \frac{P_s}{T}\left[1 + P_s\left(57.90\times10^{-8} - \frac{9.325\,0\times10^{-4}}{T} + \frac{0.258\,44}{T^2}\right)\right] \tag{1.23}$$

and the density factor for water vapor, D_w, is

$$D_w = \frac{P_w}{T}\left\{\left(-2.373\,21\times10^{-3} + \frac{2.233\,66}{T} - \frac{710.792}{T^2} + \frac{7.751\,41\times10^4}{T^3}\right)\right.$$

$$\left.\times(P_w + 3.7\times10^{-4}P_w^2) + 1\right\} \tag{1.24}$$

where

$$P = \text{total atmospheric pressure (mb)}$$

$$= \text{pressure in mm Hg} \times 1.333\,224$$

$$P_w = \text{partial water vapor pressure (mb)}$$

$$P_s = \text{partial pressure of dry air (mb)}$$

$$= P - P_w$$

$$T = \text{absolute temperature (°K)}$$

$$= \text{temperature °C} + 273.15\,.$$

```
(* Meteorological Properties of Air *)
eq523=ew-0.000662 p (t-tp)
eq524=eice-0.000583 p (t-tp)
eq527=(1.0007 + (3.46*10^(-6)*p))6.1121 Exp[17.502 tp/(240.97 + tp)]
eq528=(1.0003 + (4.18*10^(-6)*p))6.1115 Exp[22.452 tp/(272.55 + tp)]
pw=eq527 h/100
pwater[p_,t_,h_]=pw

(* Gravity Correction *)
g[phi_,z_]=-(3.085462 10^-4 +2.27 10^-7 Cos[2 phi] )z +
(7.254 10^-11 + 1.0 10^-13 Cos[2 phi])z^2 -
(1.517 10^-17+ 6 10^-20 Cos[2 phi])z^3

(* Group Index of Refraction for Air *)
eqa10=((1646386.0( (238.0185 + sigma^2)/(238.0185- sigma^2)^2)+
    47729.9((57.362 + sigma^2)/(57.362-sigma^2)^2))ds) +
   ((6487.31 + 174.174sigma^2-3.55750sigma^4 + 0.61957sigma^6)dw)
eqa4=ps/tk(1+ps(57.90 10^(-8) - 9.3250 10^(-4)/tk + 0.25844/tk^2))
eqa5=pw/tk(1+pw(1+(3.7 10^(-4) )pw) (-2.37321 10^(-3) +2.23366/tk -
     710.792/tk^2 + 7.75141 10^4/tk^3))
sigma=1/lambda
lambda=0.780
tp=t
tk=t+273.15
ps=p-pw
ds=eqa4
dw=eqa5
n=eqa10 10^(-8) +1
n[p_,t_,h_]=N[eqa10 10^{-8} +1, 12]
wave[p_,t_,h_]=N[2.99792458 10^{8}/(1500.0 10^{6} 2.0
(eqa10 10^{-8} +1)), 12]

dndt[p_,t_,h_]=D[n,t]
dndp[p_,t_,h_]=D[n,p]
dndh[p_,t_,h_]=D[n,h]

(* Group Index of Refraction for Glass *)
eq106=(a0 +a1 lambda^2 +a2 lambda^(-2) +a3 lambda^(-4) +a4 lambda^(-6)
+a5 lambda^(-8) )^(1/2)
eq107=eq106 - D[eq106,lambda] lambda

(* Schott BK 7 Glass *)
a0=2.2718929
a1=-1.0108077 10^(-2)
a2=1.0592509 10 ^(-2)
a3=2.0816965 10^(-4)
a4=-7.6472538 10^(-6)
a5=4.9240991 10^(-7)
```

Figure 1.1: Mathematica Program REFRACT.EQ

From equation (A.10), the group refractive index is

$$\begin{aligned} n_g &= 1 + \left(1\,646\,386.0\frac{238.018\,5 + \sigma^2}{(238.018\,5 - \sigma^2)^2} + 47\,729.9\frac{57.362 + \sigma^2}{(57.362 - \sigma^2)^2}\right) 10^{-8}\, D_s \\ &\quad + \left(6\,487.31 + 174.174\sigma^2 - 3.557\,50\sigma^4 + 0.619\,57\sigma^6\right) 10^{-8}\, D_w \end{aligned} \tag{1.25}$$

where

$$\begin{aligned} \sigma &= 1/\lambda\ (\mu\text{m})^{-1} \\ n_g &= \text{group refractive index.} \end{aligned}$$

For $\lambda = 0.780$ microns,

$$n_g = 1 + 7.96918 \times 10^{-5}\, D_s + 6.76673 \times 10^{-5}\, D_w. \tag{1.26}$$

1.5.1 Example Group Wavelength in Air

The group wavelength in air of a laser modulated at 1500.000 MHz is

$$\lambda_a = \frac{c}{n_g f} \tag{1.27}$$

$$= \frac{2.997\,924\,58 \times 10^8}{1500.000 \times 10^6\, n_g}\ \text{m} \tag{1.28}$$

$$= \frac{0.199\,861\,638\,7}{n_g}\ \text{m}. \tag{1.29}$$

At 20 °C, 933 mb, and 50% relative humidity

$$\lambda_a = 0.199\,811\ \text{m}. \tag{1.30}$$

1.6 Refractometer Measurement of n_g

The best method of measuring the group refractive index is with a large scale refractometer. This can be done by a direct measurement of phase over a calibrated fixed distance. From equation 5.17,

$$n_g = \frac{c}{2(D_i - D_0)f}\left(n_i - n_0 + \frac{\tilde{\phi}_i}{2\pi}\right). \tag{1.31}$$

In order to obtain representative values of n_g accurate to better than one part per million, $D_i - D_0$ must be as long as possible, and also known to the same accuracy. For example, for $D_i - D_0 = 100$ m, a measurement of n_g accurate to one part per million would require an absolute length standard of $D_i - D_0$ to 100 μm.

This is not practical for outdoor measurements, and it would be very difficult to obtain the required length in an environmental chamber! However, the derivative of $\tilde{\phi}$ with respect to n_g is a constant. Therefore, if $\tilde{\phi}$ and n_g can be calibrated at a single point, and the slope of the line can be measured, the relationship between $\tilde{\phi}$ and n_g is known for all conditions. Thus a calibrated refractometer path can be used to find n_g which is then used for the calculations for laser measurements of unknown length.

$$\frac{\partial \tilde{\phi}_i}{\partial n_g} = \frac{4\pi f}{c}(D_i - D_0) \tag{1.32}$$

or

$$\frac{\partial n_g}{\partial \tilde{\phi}_i} = \frac{c}{4\pi(D_i - D_0)f}. \tag{1.33}$$

This can be measured with the required accuracy with the only assumption that the distance $D_i - D_0$ remains constant. For example, for $D_i - D_0 = 100$ m

$$\Delta\tilde{\phi}_i = 6283\Delta n_g \text{ radians}. \tag{1.34}$$

For $\Delta n_g = 1 \times 10^{-6}$, $\Delta\tilde{\phi}_i = 6.28$ mrad. This is well within the accuracy of the phase measurement, and would only be limited by the stability of the atmospheric conditions.

The slope of a plot of $\tilde{\phi}_i$ vs n_g can be calculated from equation 1.32. If a careful measurement of $n_g(t_0, h_0, p_0)$ and $\tilde{\phi}(t_0, h_0, p_0)$ is obtained, e.g., by measuring the temperature, humidity, and pressure on a series of cold still nights and calculating n_g from equation 1.26, the plot of $\tilde{\phi}_i$ vs n_g would be completely defined. At any other set of conditions, n_g can be calculated from a measurement of $\tilde{\phi}_i$ as

$$n_g(t,h,p) = n_g(t_0,h_0,p_0) + \frac{\partial n_g}{\partial \tilde{\phi}_i}[\phi(t,h,p) - \phi(t_0,h_0,p_0)] \tag{1.35}$$

$$= n_g(t_0,h_0,p_0) + \frac{c}{4\pi(D_i - D_0)f}[\tilde{\phi}(t,h,p) - \tilde{\phi}(t_0,h_0,p_0)]. \tag{1.36}$$

From equation 1.36, n_g is then substituted into equation 5.18. The only assumption is that n_g for the refractometer is the same as the n_g for the unknown measurement path.

1.6.1 Sensitivity of n_g

The error in n_g due to error in $D_i - D_0$ can be calculated from the sensitivity of n_g

$$\frac{\partial n_g}{\partial(D_i - D_0)} = \frac{-c}{4\pi(D_i - D_0)^2 f}[\tilde{\phi}(t,h,p) - \tilde{\phi}(t_0,h_0,p_0)] \tag{1.37}$$

$$\Delta n_g = \frac{-c}{4\pi(D_i - D_0)^2 f}[\tilde{\phi}(t,h,p) - \tilde{\phi}(t_0,h_0,p_0)]\Delta(D_i - D_0). \tag{1.38}$$

For $D_i = 100$ meters, a range of phase of 0.5 radians (80 degrees °C), and an error in $D_i - D_0 = 25$ mm

$$\Delta n_g = 1.98 \times 10^{-8} \tag{1.39}$$

or well under a part per million.

1.6.2 Calibration of Refractometer

A series of simultaneous measurements of $\tilde{\phi}$, t, p, and h were made. Two people were stationed in the field, in telephone communications with someone stationed at the ZIY computer console, to take simultaneous temperature readings. The humidity was measured using a sling psychrometer. The atmospheric pressure was measured using a calibrated aneroid barometer.

For each set of data, five dry bulb temperatures were measured at the weather station box at the base of the 150' tower and under the panel experiment. Certified thermometers were suspended in free air and read, at the cue from the computer operator, with a cathetometer at the panels and with the Topcon at the weather station. It is interesting to note that the temperature is very dynamic, varying by as much as 0.5°C over one minute. The numbers were recorded, along with the $\tilde{\phi}$, by the computer operator. The data was then plotted and fitted to find a best fit of $n_g(t_0, h_0, p_0)$ and $\tilde{\phi}(t_0, h_0, p_0)$.

The distance D_i was measured using the Topcon electronic distance measurement instrument. The distance D_0 was measured in the calibration lab as part of the calibration procedure.

1.7 Group Refractive Index for Glass

A detailed treatment of the group refractive index in glass is given in reference [24], section 10.2.3. From equation 10.6,

$$n^2 = A_0 + A_1\lambda^2 + A_2\lambda^{-2} + A_3\lambda^{-4} + A_4\lambda^{-6} + A_5\lambda^{-8} \tag{1.40}$$

where

$$\lambda = \text{wavelength } (\mu m) \tag{1.41}$$

From equation 10.7, the group refractive index, n_g, is

$$n_g = n - \lambda\frac{d\,n}{d\,\lambda} \tag{1.42}$$

or

$$n_g = n - \frac{1}{n}\left(A_1\lambda^2 - A_2\lambda^{-2} - 2A_3\lambda^{-4} - 3A_4\lambda^{-6} - 4A_5\lambda^{-8}\right). \tag{1.43}$$

1.7.1 BK 7 Glass

For Schott BK 7 glass,

$$\begin{aligned} A_0 &= 2.2718929 \\ A_1 &= -1.0108077 \times 10^{-2} \\ A_2 &= 1.0592509 \times 10^{-2} \\ A_3 &= 2.0816965 \times 10^{-4} \\ A_4 &= -7.6472538 \times 10^{-6} \\ A_5 &= 4.9240991 \times 10^{-7}. \end{aligned} \tag{1.44}$$

At 0.780 μm,

$$n = 1.511186 \tag{1.45}$$

$$n_g = 1.527463, \tag{1.46}$$

or a difference of 16277 ppm. The group wavelength in BK 7 glass of a laser modulated at 1500.000 MHz is

$$\begin{aligned} \lambda_g &= \frac{c}{n_g f} \\ &= 0.130\,845 \text{ m} \end{aligned} \tag{1.47}$$

$$\frac{\lambda_g}{2} = 65.422 \text{ mm}. \tag{1.48}$$

1.8 Error Analysis

1.8.1 Sensitivity of n_g

Using the Mathematica program in Figure 1.1, the sensitivity of n_g to any of the variables is easily calculated. For example, at 20 °C, 933 mb (700 mm Hg), and 50% relative humidity,

$$n_g = 1.000\,253\,24 \tag{1.49}$$

$$\frac{\partial n_g}{\partial t} = -0.895 \times 10^{-6} \text{ /°C} \tag{1.50}$$

$$\frac{\partial n_g}{\partial p} = 0.272 \times 10^{-6} \text{ /mb} \quad (1.51)$$

$$\frac{\partial n_g}{\partial h} = -0.0096 \times 10^{-6} \text{ /\%}h \quad (1.52)$$

$$\frac{\partial n_g}{\partial P_w} = -4.09 \times 10^{-8} \text{ /mb.} \quad (1.53)$$

Chapter 2

Laser Pointing and Tracking

2.1 Coordinate System

In order to point the lasers to arbitrary three-dimensional coordinates, it is necessary to establish a number of coordinate systems and the transformation equations. The fundamental coordinate system is the ground based (x, y, z) Cartesian coordinates with the x, y origin at the center of the pintle bearing, and the reference elevation at the center of a 0.750 inch tooling ball on laser monument ZY103 with; x pointing east, y pointing north, and z pointing up—as defined on C35102M081B–with a refinement. All of the metrology work uses the NAD83 coordinate system directions. The details are included in GBT Memo 223[29]. The coordinates for the center of the GBT were taken from the STAR*NET NAD83 reduction. The grid scale factor and curvature of the earth were then corrected for a local Cartesian coordinate system. These corrected coordinates were then used in a local (Cartesian) reduction for GBT surveys such as feed arm surveys.

The details of establishing this coordinate system, deflections of the vertical, convergence angles, and curvature of the earth problems will be treated in another section. For this discussion, assume everything has been corrected to an ideal cartesian coordinate system.

2.2 Coordinate Transformations

Each rangefinder is modeled in a spherical coordinate system as a function of two 100 000 count encoders. A coordinate in the (x, y, z) system must be transformed to the laser mirror spherical coordinate system and ultimately into azimuth and elevation mirror encoder counts. This can be thought of as a series of 6 transformations.

1. A linear translation from the (x, y, z) origin to the center of the laser monument 0.7500" ball, Kelvin mount fixed point.
2. A linear rotation of the (x, y, z) axes into the laser monument axes as defined on D35420M051 where: z is fixed by the line connecting the fixed point and the v-block; y is defined as the normal to the plane of the fixed point, v-block, and flat; and x is orthogonal to z and y.
3. A linear translation from the Kelvin mount fixed point to the intersection of the mirror azimuth and elevation axes.
4. A linear rotation where: z is along the axis of the azimuth bearings, x is in the plane of the Kelvin mount, and y is orthogonal to z and x.
5. A transformation from Cartesian coordinates to spherical coordinates, as defined on D35420M051.
6. A transformation from spherical coordinates (r, θ, ϕ) to encoder counts (r, N_a, N_e).

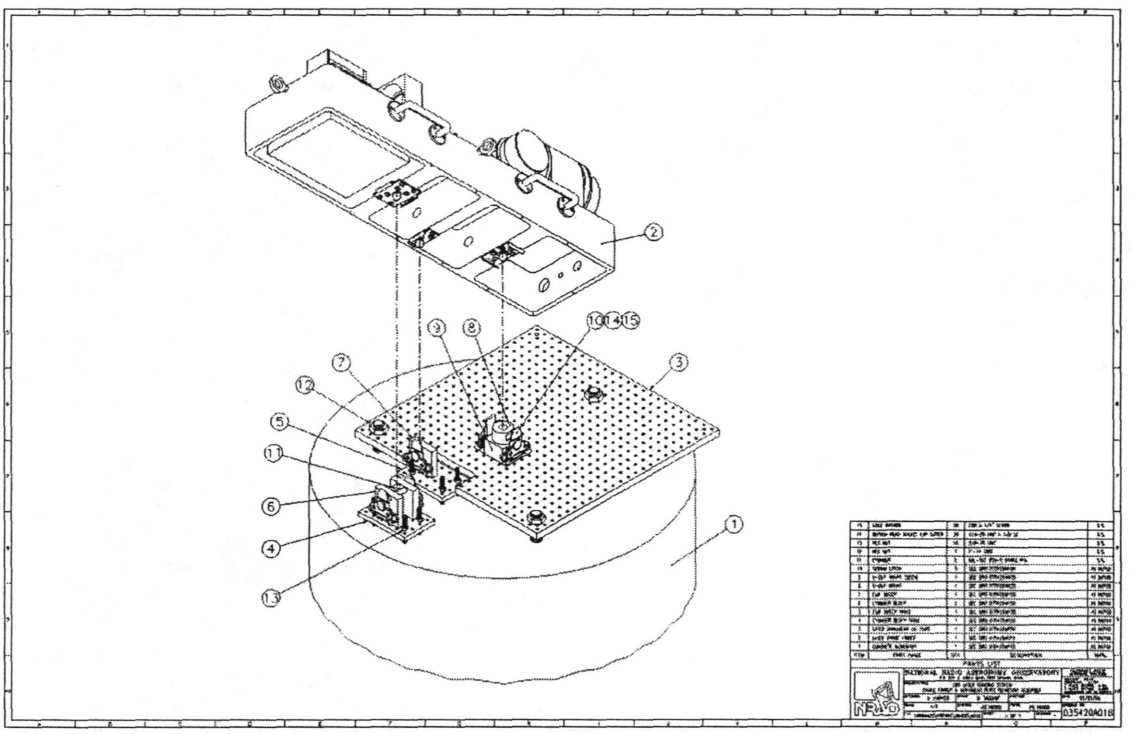

Figure 2.1: Kelvin clamp mounting.

Notice that transformations 1 and 2 are purely functions of fixed locations and orientations for the ground based lasers. These transformations can be defined from a survey of the laser monument coordinates and direction vectors. In the case of GBT mounted lasers, the coordinates and direction vectors will be functions of the azimuth and elevation of the telescope as a first approximation, but higher order corrections will be required to establish true baselines for trilateration calculations. Transformations 3 and 4 are purely functions of the mirror mechanical system. These transformations can be defined from autocollimator and mechanical measurements in the calibration lab. Transformation 5 is purely mathematical. Transformation 6 is a function of the encoder resolution and the mechanical location of the encoder index. This transformation can be defined from autocollimator measurements in the calibration lab.

In order to facilitate laser replacement and provide a mathematical framework for handling the problem of lasers mounted in a moving coordinate system on the GBT feed arm, it is desirable to maintain the transformations as these 6 distinct components, as opposed to calibrating each laser in the field and doing a linear regression of encoder counts as a function of (x, y, z), as was done in the early experimental work.

2.2.1 Integration of Survey Measurements

Step 1

The location of the fixed point of laser monument i with respect to the survey origin (bench mark) can be described by the vector $\vec{R}_i$ (R-vector). The location of any other coordinate $\vec{R}_j$ as seen from laser location $\vec{R}_i$ is

$$\vec{R}_{ij} = \vec{R}_j - \vec{R}_i. \tag{2.1}$$

In matrix notation this can be expressed as

$$\begin{pmatrix} r_{ij_x} \\ r_{ij_y} \\ r_{ij_z} \end{pmatrix} = \begin{pmatrix} r_{j_x} \\ r_{j_y} \\ r_{j_z} \end{pmatrix} - \begin{pmatrix} r_{i_x} \\ r_{i_y} \\ r_{i_z} \end{pmatrix}. \tag{2.2}$$

Laser pointing requirements for measurements of the laser monuments ($\vec{R}_i$) and retroreflectors ($\vec{R}_j$) will not require extremely high accuracy (± 5 mm), but stable bench marks will be required to locate the GBT coordinate system. It is assumed that a conventional total station surveying instrument will be used for surveying the locations. For trilateration calculations however, the laser locations must be known to an extremely high accuracy (< 1 ppm).

Step 2

The ground based lasers are oriented around the GBT coordinate origin at a radius of approximately 120 meters. Due to the mechanical design of the laser mirror system, the Kelvin mounts point radially toward the GBT coordinate system origin (pintle bearing). In order to correct for the laser monument orientation, the GBT coordinate system must be rotated into the Kelvin mount direction vectors. This transformation can be expressed in matrix notation as a 3×3 matrix where the matrix elements are the cosine of the angles between the two coordinate systems [30, 31].

The Kelvin mount coordinate system will be called $\hat{R}_{ij}$ (R-hat), i.e.,

$$\begin{pmatrix} \hat{r}_{ij_x} \\ \hat{r}_{ij_y} \\ \hat{r}_{ij_z} \end{pmatrix} = \begin{pmatrix} \gamma_{11} & \gamma_{12} & \gamma_{13} \\ \gamma_{21} & \gamma_{22} & \gamma_{23} \\ \gamma_{31} & \gamma_{32} & \gamma_{33} \end{pmatrix} \left\{ \begin{pmatrix} r_{j_x} \\ r_{j_y} \\ r_{j_z} \end{pmatrix} - \begin{pmatrix} r_{i_x} \\ r_{i_y} \\ r_{i_z} \end{pmatrix} \right\}. \tag{2.3}$$

For the ground based laser system, this transforms into $\hat{R}_z$ pointing toward the GBT origin, $\hat{R}_y$ pointing up, and $\hat{R}_x$ pointing in the GBT $x - y$ plane in a right-handed coordinate system.

A rotation transformation is an orthogonal transformation. As a result of the orthogonal transformation properties, the nine γ matrix elements are not independent. In fact, in the general case, there are only three independent matrix elements. The most convenient way to calculate the matrix elements is to use the Euler angles.

It can be shown that the γ (gamma) matrix can be calculated, from measurements using a surveying instrument and a precision level, and 4 matrices which are constants or functions of a single measurement. For the ground based lasers,

$$\begin{pmatrix} \gamma_{11} & \gamma_{12} & \gamma_{13} \\ \gamma_{21} & \gamma_{22} & \gamma_{23} \\ \gamma_{31} & \gamma_{32} & \gamma_{33} \end{pmatrix} = \tag{2.4}$$
$$\begin{pmatrix} 1 & 0 & 0 \\ 0 & \cos\alpha_3 & \sin\alpha_3 \\ 0 & -\sin\alpha_3 & \cos\alpha_3 \end{pmatrix} \begin{pmatrix} \cos\alpha_2 & \sin\alpha_2 & 0 \\ -\sin\alpha_2 & \cos\alpha_2 & 0 \\ 0 & 0 & 1 \end{pmatrix} \begin{pmatrix} \cos\alpha_1 & 0 & -\sin\alpha_1 \\ 0 & 1 & 0 \\ \sin\alpha_1 & 0 & \cos\alpha_1 \end{pmatrix} \begin{pmatrix} 1 & 0 & 0 \\ 0 & 0 & 1 \\ 0 & -1 & 0 \end{pmatrix}$$

or

$$\begin{pmatrix} \gamma_{11} & \gamma_{12} & \gamma_{13} \\ \gamma_{21} & \gamma_{22} & \gamma_{23} \\ \gamma_{31} & \gamma_{32} & \gamma_{33} \end{pmatrix} = \tag{2.5}$$
$$\begin{pmatrix} \cos(\alpha_1)\cos(\alpha_2) & \sin(\alpha_1)\cos(\alpha_2) & \sin(\alpha_2) \\ -\cos(\alpha_1)\sin(\alpha_2)\cos(\alpha_3) + \sin(\alpha_1)\sin(\alpha_3) & -\sin(\alpha_1)\sin(\alpha_2)\cos(\alpha_3) - \cos(\alpha_1)\sin(\alpha_3) & \cos(\alpha_2)\cos(\alpha_3) \\ \sin(\alpha_1)\cos(\alpha_3) + \cos(\alpha_1)\sin(\alpha_2)\sin(\alpha_3) & -\cos(\alpha_1)\cos(\alpha_3) + \sin(\alpha_1)\sin(\alpha_2)\sin(\alpha_3) & -\cos(\alpha_2)\sin(\alpha_3) \end{pmatrix}.$$

Where α_1 is the angle between south $(-y)$ and the $\hat{z}$ direction vector, measured as a positive rotation (ccw) about the $\hat{y}$ direction vector. Surveyors define a positive azimuth as clockwise from north, therefore

$$\alpha_1 = \pi - \text{azimuth} \tag{2.6}$$

where azimuth is the survey azimuth of the line connecting the fixed point and the vee block. Angle α_2 is the fine correction for tipping of the Kelvin mount about the $\hat{z}$ direction vector, and α_3 is the fine correction for tipping of the Kelvin mount about the $\hat{x}$ direction vector.

Angle α_1 can be determined using the surveying instrument mounted on a Kelvin mount plate that was calibrated in the calibration lab, in conjunction with Polaris observations and coordinates of monuments. This is explained in detal in GBT Memo 229[32]. Angles α_2 and α_3 can be determined by placing a surface plate and three 0.7500" balls on the Kelvin mount and using a precision level to find the plane of the mount. If the laser monument is greater than about 30 meters from the coordinate origin, the gravitational vector should be corrected for the curvature of the earth [33].

All of the measurements and data for each monument and control panel are tabulated on the Laser Monument Calibration Report[34] in Figure 2.2.

2.2.2 Calibration Lab Measurements

Step 3

The Green Bank Metrology Lab is equipped to completely calibrate and model the as-built instruments, as documented in GBT Memo 224[35]. A detailed report on the calibration procedures was written by John Shelton and Jason Ray[36], with revisions by John and Troy Fakes documented in Calibration Lab Record Book Number 4, p.91-94[37].

The coordinate system with the origin at the mirror center and the same direction vectors as in the $\hat{R}$ system will be called the $\check{R}$ (R-check) coordinate system, where

$$\begin{pmatrix} \check{r}_{ij_x} \\ \check{r}_{ij_y} \\ \check{r}_{ij_z} \end{pmatrix} = \begin{pmatrix} \hat{r}_{ij_x} \\ \hat{r}_{ij_y} \\ \hat{r}_{ij_z} \end{pmatrix} - \begin{pmatrix} \Delta x \\ \Delta y \\ \Delta z \end{pmatrix}. \tag{2.7}$$

LASER MONUMENT CALIBRATION REPORT

ZY_____ DATE_____ INITIALS_____

ZP NUMBER	
CONTROL PANEL	
ETHERNET ADDRESS	
IP ADDRESS	
x	
y	
z	
azimuth	
α_1 (π−azimuth)	
α_2 (rotation about $\hat{z}$)	
α_3 (rotation about $\hat{x}$)	
LATITUDE	
LONGITUDE	
ELEVATION	
WV X	
WV Y	
WV Z	
γ_{11}	
γ_{12}	
γ_{13}	
γ_{21}	
γ_{22}	
γ_{23}	
γ_{31}	
γ_{32}	
γ_{33}	

NOTES:

Figure 2.2: Laser Monument Calibration Report, rev 1/20/96

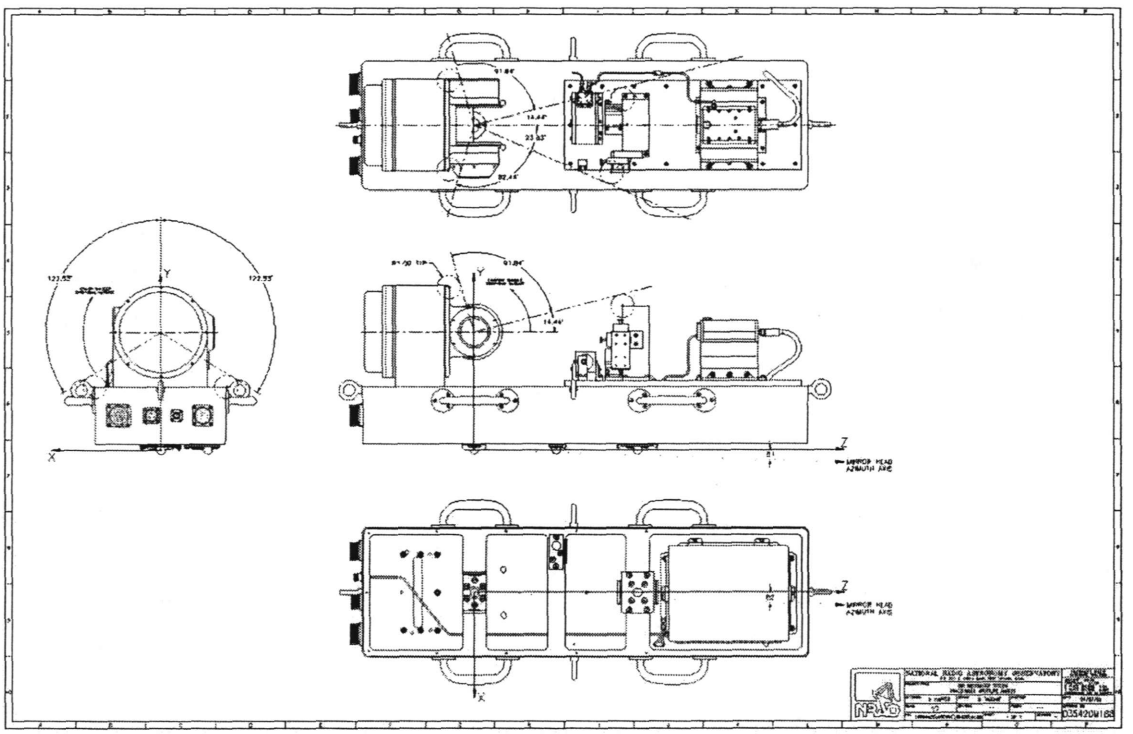

Figure 2.3: ZP axes, angles, and rotational directions.

The offset between the Kelvin mount coordinate ($\hat{R}$) origin and the mirror center coordinate ($\check{R}$) origin, $(\Delta x, \Delta y, \Delta z)$, can be measured in the calibration lab. Note that the positive direction for the Δs is along the axes from the tooling ball to the mirror, e.g., the height of the mirror axis above the tooling ball center is $+\Delta y$, offset of the mirror in the direction of the detector is $+\Delta z$, and offset of the mirror in the $+x$ direction is $+\Delta x$. The instrument is placed on calibrated (matched) v-blocks on the 8' surface plate. Using the height gage, indicators, and gage blocks, the offsets are measured and recorded.

Step 4

Due to mechanical misalignment of the mirror azimuth axis, with respect to the Kelvin mount axes, an additional rotation transformation must be performed. The coordinate system with the origin at the mirror center and the z axis along the azimuth mechanical axis will be called the $\tilde{R}$ (R-tilde) coordinate system. The x axis is defined to be in the plane of the surface plate for convenience. This can be written as

$$\begin{pmatrix} \tilde{r}_{ij_x} \\ \tilde{r}_{ij_y} \\ \tilde{r}_{ij_z} \end{pmatrix} = \begin{pmatrix} \lambda_{11} & \lambda_{12} & \lambda_{13} \\ \lambda_{21} & \lambda_{22} & \lambda_{23} \\ \lambda_{31} & \lambda_{32} & \lambda_{33} \end{pmatrix} \left\{ \begin{pmatrix} \hat{r}_{ij_x} \\ \hat{r}_{ij_y} \\ \hat{r}_{ij_z} \end{pmatrix} - \begin{pmatrix} \Delta x \\ \Delta y \\ \Delta z \end{pmatrix} \right\}. \tag{2.8}$$

The most convenient way to calculate the matrix elements is to use a set of Euler angles that are chosen in such a way as to be directly measurable with an autocollimator. A modification of the operations described on page 146 of Goldstein [30] is used. Due to the choice that the mirror $\tilde{x}$ axis be in the plane of the surface plate (Kelvin mount), the number of angles needed reduces to two, i.e., the angle β_2 between the $\hat{x}$ and $\tilde{x}$ axes (rotation about $\hat{y}$) and the angle β_1 between the $\hat{y}$ and $\tilde{y}$ axes (rotation about $\hat{x}$). Note that in some reports β_1 is called θ, and β_2 is called ϕ (sorry about that). For a rotation about the $\hat{y}$ axis, the transformation matrix is

$$\begin{pmatrix} \cos\beta_2 & 0 & -\sin\beta_2 \\ 0 & 1 & 0 \\ \sin\beta_2 & 0 & \cos\beta_2 \end{pmatrix}. \tag{2.9}$$

Notice that this rotates the $\hat{x}$ axis into the $\tilde{x}$ axis in the plane of the surface plate. A rotation about the $\hat{x}$ axis is described by the following transformation matrix

$$\begin{pmatrix} 1 & 0 & 0 \\ 0 & \cos\beta_1 & \sin\beta_1 \\ 0 & -\sin\beta_1 & \cos\beta_1 \end{pmatrix}. \tag{2.10}$$

For small angles, the combination of operations yields the λ rotation transformation matrix, where

$$\begin{aligned} \begin{pmatrix} \lambda_{11} & \lambda_{12} & \lambda_{13} \\ \lambda_{21} & \lambda_{22} & \lambda_{23} \\ \lambda_{31} & \lambda_{32} & \lambda_{33} \end{pmatrix} &= \begin{pmatrix} 1 & 0 & 0 \\ 0 & \cos\beta_1 & \sin\beta_1 \\ 0 & -\sin\beta_1 & \cos\beta_1 \end{pmatrix} \begin{pmatrix} \cos\beta_2 & 0 & -\sin\beta_2 \\ 0 & 1 & 0 \\ \sin\beta_2 & 0 & \cos\beta_2 \end{pmatrix} \\ &= \begin{pmatrix} \cos\beta_2 & 0 & -\sin\beta_2 \\ \sin\beta_1\sin\beta_2 & \cos\beta_1 & \sin\beta_1\cos\beta_2 \\ \cos\beta_1\sin\beta_2 & -\sin\beta_1 & \cos\beta_1\cos\beta_2 \end{pmatrix}. \end{aligned} \tag{2.11}$$

Using a combination of granite angle and straight edge standards, and autocollimator mirror angle standards, the autocollimator is aligned with the Kelvin mount $\hat{z}$ axis on the surface plate. Looking into the laser mirror with the autocollimator, the elevation axis is adjusted (using the computer control system) until the reflection is stationary in that axis for 180° flips of the azimuth. The laser mirror adjustment screws are then adjusted for the other axis. After several iterations

between adjusting the elevation and mirror adjustment screws, the autocollimator reflection should remain fixed as the azimuth axis is rotated.

The two dimensional displacement of the autocollimator reflection is the angle between the $\hat{z}$ and $\tilde{z}$ axes. For small angles, angle β_2 is read directly as the x component of the displacement between the cross and target and angle β_1 is approximately the y component of the displacement between the cross and target.

Summary of Coordinate Transformations

Transformations 1–4 can be written as

$$\begin{pmatrix} \tilde{r}_{ij_x} \\ \tilde{r}_{ij_y} \\ \tilde{r}_{ij_z} \end{pmatrix} = \begin{pmatrix} \lambda_{11} & \lambda_{12} & \lambda_{13} \\ \lambda_{21} & \lambda_{22} & \lambda_{23} \\ \lambda_{31} & \lambda_{32} & \lambda_{33} \end{pmatrix} \left\{ \left\{ \begin{pmatrix} \gamma_{11} & \gamma_{12} & \gamma_{13} \\ \gamma_{21} & \gamma_{22} & \gamma_{23} \\ \gamma_{31} & \gamma_{32} & \gamma_{33} \end{pmatrix} \left\{ \begin{pmatrix} r_{j_x} \\ r_{j_y} \\ r_{j_z} \end{pmatrix} - \begin{pmatrix} r_{i_x} \\ r_{i_y} \\ r_{i_z} \end{pmatrix} \right\} \right\} - \begin{pmatrix} \Delta x \\ \Delta y \\ \Delta z \end{pmatrix} \right\}. \tag{2.12}$$

2.3 Conversion to Spherical Coordinates

Step 5

Due to the mechanical design of the laser mirror, it is convenient to convert to spherical coordinates $(|\tilde{r}_{ij}|, \Theta, \Phi)$ as defined by drawing D35420M051. Θ is a positive rotation of the azimuth encoder (using right hand rule) about the $\tilde{z}$ axis and Φ is a positive rotation of the elevation encoder. For $\Theta = 0$, the laser beam is in the $\tilde{x} - \tilde{z}$ plane, i.e., the elevation shaft goes through the $\tilde{y}$ axis with the encoder down. For $\Phi = 0$, the laser beam points down the $\tilde{z}$ axis.

The spherical coordinates are calculated from the $\tilde{R}_{ij}$ components as

$$|\tilde{r}_{ij}| = \left(\tilde{r}^2_{ij_x} + \tilde{r}^2_{ij_y} + \tilde{r}^2_{ij_z} \right)^{1/2} \tag{2.13}$$

$$\Theta = \tan^{-1}\left(\frac{\tilde{r}_{ij_y}}{\tilde{r}_{ij_x}} \right) \tag{2.14}$$

$$\Phi = \cos^{-1}\left(\frac{\tilde{r}_{ij_z}}{|\tilde{r}_{ij}|} \right), \tag{2.15}$$

or

$$\tilde{x} = |\tilde{r}_{ij}| \sin\Phi \cos\Theta \tag{2.16}$$

$$\tilde{y} = |\tilde{r}_{ij}| \sin\Phi \sin\Theta \tag{2.17}$$

$$\tilde{z} = |\tilde{r}_{ij}| \cos\Phi. \tag{2.18}$$

Due to mechanical stops on the azimuth, and the choice of coordinates

$$-\pi/2 \leq \Theta < 3\pi/2 \tag{2.19}$$

$$0 \leq \Phi \leq \pi. \tag{2.20}$$

2.4 Conversion to Encoder Counts

Step 6

The incremental encoders on the mirror are 100 000 counts/revolution with a once/revolution index pulse. The encoder count as a function of Θ and Φ for a mirror in the proper orientation will be

$$N_a = \frac{10^5\ \Theta}{2\pi} + N_{a_0} \tag{2.21}$$

$$N_e = \frac{10^5\ \Phi}{4\pi} + N_{e_0} \tag{2.22}$$

where N_a and N_e are the azimuth and elevation encoder counts and N_{a_0} and N_{e_0} are the zero offsets of the encoders, i.e., the encoder counts at $\Theta = 0$ and $\Phi = 0$.

The zero offsets of the encoders are measured using the autocollimator as described in step 4. The elevation zero offset, N_{e_0} when $\Phi = 0$, is the elevation encoder position where the laser points along the $\tilde{z}$ axis, i.e., the autocollimator reflection is stationary for rotations of the azimuth axis. The azimuth zero offset, N_{a_0} when $\Theta = 0$, is found by setting $\Phi = 90°$ (mirror tilted 45°) and sighting into an autocollimator mirror located on the $\tilde{x}$ axis. When the y displacement of the autocollimator target is zeroed, the beam points along the $\tilde{x}$ axis. This encoder value is N_{a_0}.

For calibration, it is sometimes useful to autocollimate off the mirror from a target location, e.g., using a laser located on monument 101 looking into the mirror on monument 100. In this case the encoder positions are calculated the same way except the elevation is modified by a factor of two

$$N_e = \frac{10^5\ \Phi}{2\pi} + N_{e_0}. \tag{2.23}$$

It is also useful to shoot the retroreflector built into the back side of the mirror. For this case,

$$N_e = \frac{10^5\ \Phi}{2\pi} + N_{e_0} + \frac{10^5}{2}. \tag{2.24}$$

Note that the combination of azimuth and elevation angles for the mirror are not unique, i.e., there are two combinations that point the same. For convience, I call the alternate combination the prime (′) pointing. For calibration purposes, it can be useful to measure using both configurations in order to extract instrumental errors–much like surveyors do by plunging the instrument. For example, if the mirror is not exactly on the mechanical axis of rotation, the autocolimate distance will not be the same in both configurations, and the difference between the two will be twice the offset error. The diference between distances to the back retroreflector are an indication of the offset between the azimuth and elevation mechanical axes.

The encoder settings for the prime pointing is easily derived since the azimuth is simply rotated by 180 degrees, and the magnitude of the elevation offset from N_{e0} is the same, except the direction of rotation is reversed. Therefore

$$N'_a = N_a + 50\ 000 \tag{2.25}$$

and

$$N'_e = 2N_{e0} - N_e. \tag{2.26}$$

Of course checks must be made to ensure the allowed range range of N_a in order to avoid hitting the mechanical stop.

All of the calibration lab data is recorded on the Laser Mirror Assembly Calibration Report shown in Figure 2.4.

2.5 Example Problem

Step 1

An example problem will serve to illustrate the coordinate transformation process. A survey of the laser test range monuments and test panel retroreflector locations was done using the Topcon GTS 301 total station. The instrument was mounted on a tribrach centered on ZBG4, which was defined as the x and y coordinate origin. The y coordinate origin was defined as the center of the 0.7500" tooling ball on ZY2 monument. The coordinate system was defined in the same directions

LASER MIRROR ASSEMBLY CALIBRATION REPORT

ZP_____ DATE_____ INITIALS_____

LASER NUMBER	
DETECTOR NUMBER	
HEAD NUMBER	
OSCILLATOR NUMBER	
LEAKAGE SIGNAL	
D_0	
Δx	
Δy	
Δz	
β_1 rotation about x (θ)	
β_2 rotation about y (ϕ)	
N_{a0}	
N_{e0}	
AZ LOW LIMIT	
AZ HIGH LIMIT	
AZM ZRG	
ABV 0	
ABA 0	
FKP 0	
FKI 0	
FKD 0	
FIL 0	
FSI 0	
ERL 0	
ELV ZRG	
ABV 1	
ABA 1	
FKP 1	
FKI 1	
FKD 1	
FIL 1	
FSI 1	
ERL 1	
λ_{11}	
λ_{12}	
λ_{13}	
λ_{21}	
λ_{22}	
λ_{23}	
λ_{31}	
λ_{32}	
λ_{33}	

NOTES:

Figure 2.4: Laser Mirror Assembly Calibration Report, rev 1/20/96

as C35102M081. True north was established with an accuracy of around ±5 seconds from Polaris observations as described in references [38] and [39].

A 3.5000" K&E sphere mounted target was used for measuring angles, and a hollow retroreflector (also mounted in a 3.5000" sphere) was used for all distance measurements. The sphere was centered over the 0.7500" ball using a 3-ball chuck (see drawing D35420M085) which was leveled with a bubble level to an accuracy of around one arcminute.

ZY2 and ZY3 laser mounts were approximately leveled using a precision granite flat plate resting on three 0.7500" balls in the laser Kelvin mount, and a machinists' level. An attempt was made to measure the elevation of ZY3 using the Pellissier H5 hydrostatic level, but the sun shining on the hose produced unrepeatable results. This will be repeated at night this summer. We also have plans to measure the spacing between ZY2 and ZY3 using ZY1 and a mirror system.

Using the Topcon, the coordinates of monument ZY3 are (5586.2, 20850.0, −5.8), where all dimensions are in mm, or

$$\begin{pmatrix} r_{ij_x} \\ r_{ij_y} \\ r_{ij_z} \end{pmatrix} = \begin{pmatrix} r_{j_x} \\ r_{j_y} \\ r_{j_z} \end{pmatrix} - \begin{pmatrix} 5586.2 \\ 20850.0 \\ -5.8 \end{pmatrix}. \tag{2.27}$$

Step 2

A tribrach was mounted on a tooling plate with three tooling balls in the same geometry as a laser mount. The assembly was placed on monument 100 in the calibration lab and weighted with a lead brick. The Kelvin mount v-block ($\hat{z}$ axis) on monument 100 has been established to be turned 90°00′00″ ±02″ from the reference line connection monument 100 to monument 102 ($\hat{x}$ axis). The Topcon azimuth was set to zero when aligned on a target centered on monument 102, i.e., the $\hat{x}$ axis. Thus an accurate azimuth with respect to the Kelvin mount v-block was established.

It was found that by releasing the lock on the azimuth before moving the instrument, we could transport the assembly to the field to make azimuth measurements, referenced to the Kelvin mount, and return to the lab with closures of the order of an arc-second.

Note: An alternate method is described in GBT Memo 229[32]. Caution must be used with both methods to avoid the tilt error described by Polasek (see p. 1196)[40].

Using this method to establish the true azimuth of the field laser mounts, The $\hat{x}$ axis of ZY3 was measured to be at an azimuth (from true north) of 32°11′50″. Note that surveyors measure azimuth in the clockwise direction from north, e.g., north=0°, east=90°. An azimuth of 32°11′50″ translates to a counter clockwise rotation (+ direction using right hand rule) about the $\hat{y}$ axis of 57°48′10″, or

$$\alpha_1 = +57°48'10'' \tag{2.28}$$

The mounts were then checked using the precision granite flat plate resting on three 0.7500" steel balls in the Kelvin mount. A split bubble Clineometer level was used to measure small rotations of the mount. ZY3 was found to be rotated −05″ about $\hat{z}$ and +30″ about $\hat{x}$, i.e.,

$$\alpha_2 = -0°00'05'' \tag{2.29}$$

$$\alpha_3 = +0°00'30''. \tag{2.30}$$

Using equation 2.6 and the Mathematica program in figure 2.5, the γ matrix (cosine of the angles between the GBT coordinate system and the Kelvin mount coordinate system) was calculated to be;

$$\begin{pmatrix} \gamma_{11} & \gamma_{12} & \gamma_{13} \\ \gamma_{21} & \gamma_{22} & \gamma_{23} \\ \gamma_{31} & \gamma_{32} & \gamma_{33} \end{pmatrix} = \begin{pmatrix} 0.532\,835 & 0.846\,218 & -0.000\,024 \\ 0.000\,135 & -0.000\,056 & 0.999\,999 \\ 0.846\,218 & -0.532\,835 & -0.000\,145 \end{pmatrix}. \tag{2.31}$$

```
(* CAL.EQ 1/20/96 *)
<<a:zytest.eq  (* get data for monument  *)
<<a:zp10.eq  (* get data for laser mirror  *)
a= {{Cos[phi],0,-Sin[phi]},{0,1,0},{Sin[phi],0,Cos[phi]}}
b={{1,0,0},{0,Cos[theta],Sin[theta]},{0,-Sin[theta],Cos[theta]}}
lambda=b.a
c={{1,0,0},{0,0,1},{0,-1,0}}
d={{Cos[alpha1],0,-Sin[alpha1]}, {0,1,0},{Sin[alpha1],0,Cos[alpha1]}}
e={{Cos[alpha2], Sin[alpha2], 0},{-Sin[alpha2], Cos[alpha2], 0},{0,0,1}}
f={{1,0,0},{0, Cos[alpha3], Sin[alpha3]},{0,-Sin[alpha3],Cos[alpha3]}}
gamma=f.e.d.c
rj:={x,y,z}
r:=lambda.((gamma.(rj-ri))-{dx,dy,dz})
rmag:=(r.r)^.5
thetaaz:=ArcTan[ r[[1]], r[[2]] ]
phiel:=ArcCos[ r[[3]]/rmag]
na[x_,y_,z_]=10^5 thetaaz/(2 Pi) + na0
ne[x_,y_,z_]=10^5 phiel/(4 Pi) + ne0
   (* return az, el encoder coordinates for pointing to location (x,y,z)
and el coordinate to autocollimate *)
enc[{x_,y_,z_}]= {{x,y,z},  N[{ 10^5 thetaaz/(2 Pi) + na0,
10^5 phiel/(4 Pi) + ne0, 10^5 phiel/(2 Pi) + ne0} ]}
coordinates = ReadList["a:coord.dat", Number, RecordLists -> True]
Do[ OutputForm[PaddedForm[  enc[coordinates[[i]]] ,{8,1}]]
>>>a:output.dat , {i,13}  ]
```

Figure 2.5: Mathematica Program CAL.EQ

```
alpha1=1.008848
alpha2=-.000024
alpha3=.000145
ri={5586.2, 20850.0, -5.8}
```

Figure 2.6: ZY3 Monument Calibration Data. Filename=A:ZY3.EQ

```
dx=-.075
dy=247.459
dz=-.762
phi=.000121
theta=-.000727
na0=-4195
ne0=-4935
```

Figure 2.7: ZP3 Mirror Calibration Data. Filename= A:ZP3.EQ

Thus the coordinates of point $\vec{R}_j$ in the $\hat{R}_{ij}$ coordinate system, as seen from ZY3, are

$$\begin{pmatrix} \hat{r}_{ij_x} \\ \hat{r}_{ij_y} \\ \hat{r}_{ij_z} \end{pmatrix} = \begin{pmatrix} 0.532\,835 & 0.846\,218 & -0.000\,024 \\ 0.000\,135 & -0.000\,056 & 0.999\,999 \\ 0.846\,218 & -0.532\,835 & -0.000\,145 \end{pmatrix} \left\{ \begin{pmatrix} r_{j_x} \\ r_{j_y} \\ r_{j_z} \end{pmatrix} - \begin{pmatrix} 5586.2 \\ 20850.0 \\ -5.8 \end{pmatrix} \right\}. \quad (2.32)$$

Step 3

Laser unit ZP3 was calibrated in the calibration lab. The mirror offsets were measured to be

$$\begin{pmatrix} \Delta x \\ \Delta y \\ \Delta z \end{pmatrix} = \begin{pmatrix} -0.075 \\ 247.459 \\ -0.762 \end{pmatrix}. \quad (2.33)$$

Step 4

The $\hat{z}$ axis of laser unit number 3 was established on the surface plate by mounting the fixed point and v-block point in matched v-blocks (# 4346) against a straight edge. The third tooling ball was placed in a v-block (# xxxx) that was allowed to self align to the $\hat{z}$ axis straight edge. The $\hat{z}$ axis was established for the autocollimator by sighting on a granite master square (0.000 025"/6") placed against the straight edge. A 2" Starrett Croblox flat reflecting target, flat and parallel to 0.05μm, was mounted against the master square.

The laser mirror was adjusted in the mount using shims to make the mirror parallel with the elevation mechanical axis. In the final unit design, this will be adjustable. The elevation servo was adjusted to minimize motion of the autocollimator target image as the azimuth was rotated. This minimum was defined as the $\tilde{z}$ axis orientation. The elevation encoder in this position defines N_{e0} which was

$$N_{e0} = -4935. \quad (2.34)$$

The $\tilde{z}$ axis was measured to be rotated up 0°02′30″ and rotated in the plane of the surface plate towards the $\tilde{x}$ axis by 0°00′25″, i.e.,

$$\beta_2 = +0°00'25'' \quad (2.35)$$

$$\beta_1 = -0°02'30'' \quad (2.36)$$

Using equation 2.12 The λ rotation matrix elements are

$$\begin{pmatrix} \lambda_{11} & \lambda_{12} & \lambda_{13} \\ \lambda_{21} & \lambda_{22} & \lambda_{23} \\ \lambda_{31} & \lambda_{32} & \lambda_{33} \end{pmatrix} = \begin{pmatrix} 0.999\,999 & 0 & -0.000\,121 \\ 0 & 0.999\,999 & -0.000\,727 \\ 0.000\,121 & 0.000\,727 & 0.999\,999 \end{pmatrix}. \quad (2.37)$$

Transformations 1–4 for laser unit 3 on monument ZY3 are

$$\begin{pmatrix} \tilde{r}_{ij_x} \\ \tilde{r}_{ij_y} \\ \tilde{r}_{ij_z} \end{pmatrix} = \begin{pmatrix} 0.999\,999 & 0 & -0.000\,121 \\ 0 & 0.999\,999 & -0.000\,727 \\ 0.000\,121 & 0.000\,727 & 0.999\,999 \end{pmatrix} \quad (2.38)$$

$$\left(\left\{ \begin{pmatrix} 0.532\,835 & 0.846\,218 & -0.000\,024 \\ 0.000\,135 & -0.000\,056 & 0.999\,999 \\ 0.846\,218 & -0.532\,835 & -0.000\,145 \end{pmatrix} \left[\begin{pmatrix} r_{j_x} \\ r_{j_y} \\ r_{j_z} \end{pmatrix} - \begin{pmatrix} 5586.2 \\ 20850.0 \\ -5.8 \end{pmatrix} \right] \right\} - \begin{pmatrix} -0.075 \\ 247.459 \\ -0.762 \end{pmatrix} \right).$$

Step 6

The master square was then approximately aligned along the $\hat{x}$ axis. The elevation mirror was increased 12 500 counts to point in the $\tilde{x}$-$\tilde{y}$ plane. The azimuth servo was then positioned to align the autocollimator into the square mounted mirror, i.e., the $\tilde{x}$ axis intersection with the surface plate ($\hat{x}$–$\hat{z}$) plane. The azimuth encoder in this position is N_{a0}. This was measured to be

$$N_{a0} = -4195. \tag{2.39}$$

2.6 Coordinate Transformation Equations for Tracking

For ground based lasers to track points on the GBT, the coordinates will be transformed from the alidade, elevation, reflector, prime focus and subreflector coordinate systems to the ground based coordinates, as defined on drawing C35102M081B. These transformations will be made by the ZIY computer based on information from the telescope model, finite element analysis, and the encoders. Each ZY laser system will then transform from the GBT ground based (X, Y, Z) coordinates to the (N_a, N_e) coordinates for the monument–laser combination.

First order correction equations are given on drawing C35102M081B (note that there is an error in R_{23} on this revision). For our purposes, it is more useful to develop the equations in terms of the astronomical azimuth instead of the arbitrary south orientation of the encoder. For this convention, the transformation from the alidade to ground is a negative rotation about the z axis for clockwise rotation, or

$$R_{ag} = \begin{pmatrix} \cos\alpha_a & \sin\alpha_a & 0 \\ -\sin\alpha_a & \cos\alpha_a & 0 \\ 0 & 0 & 1 \end{pmatrix} \tag{2.40}$$

where α_a is the astonomical azimuth measured clockwise from north.

The transform from the elevation coordinate system to the azimuth coordinate system can be performed by first rotating the elevation $-\pi/2$ about the x axis (to make the elevation z axis point horizontal at an elevation angle of 0) followed by a positive rotation about the elevation axis of α_e, and then a translation in the z direction.

$$\begin{aligned} R_{ea} &= \begin{pmatrix} 1 & 0 & 0 \\ 0 & \cos\alpha_e & -\sin\alpha_e \\ 0 & \sin\alpha_e & \cos\alpha_e \end{pmatrix} \begin{pmatrix} 1 & 0 & 0 \\ 0 & \cos -\pi/2 & -\sin -\pi/2 \\ 0 & \sin -\pi/2 & \cos -\pi/2 \end{pmatrix} \\ &= \begin{pmatrix} 1 & 0 & 0 \\ 0 & \sin\alpha_e & \cos\alpha_e \\ 0 & -\cos\alpha_e & \sin\alpha_e \end{pmatrix} \end{aligned} \tag{2.41}$$

or

$$\begin{pmatrix} X_a \\ Y_a \\ Z_a \end{pmatrix} = \left[\begin{pmatrix} 1 & 0 & 0 \\ 0 & \sin\alpha_e & \cos\alpha_e \\ 0 & -\cos\alpha_e & \sin\alpha_e \end{pmatrix} \begin{pmatrix} X_e \\ Y_e \\ Z_e \end{pmatrix} \right] + \begin{pmatrix} 0 \text{ mm} \\ 0 \text{ mm} \\ 48\ 260.000 \text{ mm} \end{pmatrix} \tag{2.42}$$

The transformation from the reflector coordinate system to the elevation coordinate system is a translation.

$$T_{re} = \begin{pmatrix} 0 \text{ mm} \\ -54\ 839.108 \text{ mm} \\ 4\ 999.990 \text{ mm} \end{pmatrix} \tag{2.43}$$

The total transformation from the reflector to the ground is

$$\begin{pmatrix} X \\ Y \\ Z \end{pmatrix} = \begin{pmatrix} \cos\alpha_a & \sin\alpha_a & 0 \\ -\sin\alpha_a & \cos\alpha_a & 0 \\ 0 & 0 & 1 \end{pmatrix} \left\{ \left[\begin{pmatrix} 1 & 0 & 0 \\ 0 & \sin\alpha_e & \cos\alpha_e \\ 0 & -\cos\alpha_e & \sin\alpha_e \end{pmatrix} \begin{pmatrix} X_r & 0 \text{ mm} \\ Y_r & + -54\,839.108 \text{ mm} \\ Z_r & 4\,999.990 \text{ mm} \end{pmatrix} \right] + \begin{pmatrix} 0 \text{ mm} \\ 0 \text{ mm} \\ 48\,260.000 \text{ mm} \end{pmatrix} \right\} \tag{2.44}$$

The first order correction equations do not take structural deformations into account—which must be done [41, 42]. It is assumed that finite element analysis models will be used to do second order repeatable corrections for the origin and direction vectors of each of the moving GBT coordinate systems. With feedback from the laser system, the finite element analysis model should be refined to the point of modeling the GBT for repeatable deformations. It is also assumed that the ground based laser system will do third order corrections to remove nonrepeatable deflections of the structure. Selection of the cardinal points the laser system uses should be dictated by the finite element analysis model in order to optimize the best fit.

2.6.1 Dynamic Tracking

It will also be necessary for the laser to track the retroreflectors as a function of time, where time is defined by IRIG sync of each computer to an accuracy on the order of 1 μs.. The derivatives of N_a and N_e are assumed to be constant over the integration period—typically 128 ms.

The ZIY will give the ZYs the projected $\vec{R}_j(t_0)$ and $\vec{R}_j(t_1)$ based on the telescope geometry, finite element analysis models, and azimuth and elevation positions and velocities from the monitor and control system. The ZY will calculate the projected encoder coordinates for times t_0 and t_1 and generate the linear approximation of $N_a(t)$ and $N_e(t)$, i.e.,

$$N_a(t) = \frac{N_a(t_1) - N_a(t_0)}{t_1 - t_0}(t - t_0) + N_a(t_0) \tag{2.45}$$

$$N_e(t) = \frac{N_e(t_1) - N_e(t_0)}{t_1 - t_0}(t - t_0) + N_e(t_0). \tag{2.46}$$

For lasers mounted on the GBT, the $\vec{R}_i$ coordinates and the γ rotation matrix elements will be functions of azimuth, elevation and vibrational amplitude and phase. It is expected that the feed arm vibrational amplitude and phase will be measured by a quadrant detector mounted on the feed arm. Another solution would be to use ground based lasers to track the feed arm in a phase lock loop filtered mode that allows the position of the arm, and thus $\vec{R}_j$ and γ to be predicted for the near future.

2.7 Sun Avoidance

As the lasers track retroreflectors, care must be taken to avoid pointing the mirror into the sun. The ZIY computer will generate a unit direction vector pointing to the sun. The ZY computers will check to make sure the mirror is not pointing in this zone. In this case, the pointing equations can be reduced to

$$\begin{pmatrix} \tilde{r}_{ij_x} \\ \tilde{r}_{ij_y} \\ \tilde{r}_{ij_z} \end{pmatrix} = \begin{pmatrix} \lambda_{11} & \lambda_{12} & \lambda_{13} \\ \lambda_{21} & \lambda_{22} & \lambda_{23} \\ \lambda_{31} & \lambda_{32} & \lambda_{33} \end{pmatrix} \begin{pmatrix} \gamma_{11} & \gamma_{12} & \gamma_{13} \\ \gamma_{21} & \gamma_{22} & \gamma_{23} \\ \gamma_{31} & \gamma_{32} & \gamma_{33} \end{pmatrix} \begin{pmatrix} r_{j_x} \\ r_{j_y} \\ r_{j_z} \end{pmatrix}. \tag{2.47}$$

Chapter 3

Distance to Coordinate Calculations

3.1 3–D Coordinate Calculation Using Trilateration

3.1.1 Minimum Calculation

[1]

For the panel experiment, three laser distances were obtained. This is the minimum data needed for the trilateration algorithm, i.e., no redundancy. A detailed treatment of the trilateration algorithm is given in section 10.1.2 of reference [43]. Assume three laser systems located at known locations $\vec{R}_1$, $\vec{R}_2$, and $\vec{R}_3$ measure the distances R_{1j}, R_{2j}, and R_{3j} to unknown point j. There exists a unique set of coordinates $(r_{j_x}, r_{j_y}, r_{j_z})$ such that

$$R_{ij}^2 = (r_{i_x} - r_{j_x})^2 + (r_{i_y} - r_{j_y})^2 + (r_{i_z} - r_{j_z})^2 \tag{3.1}$$

for $i = 1$, 2, and 3.

The problem reduces to finding a solution to this set of three nonlinear equations. The general approach is to linearize the equations and assume a value for $(r_{j_x}, r_{j_y}, r_{j_z})$. A new set of values $(\tilde{r}_{j_x}, \tilde{r}_{j_y}, \tilde{r}_{j_z})$ is found, and the average of the old and new values is substituted into the equation. The process is repeated until the old and new values converge to within a defined ϵ.

Expanding equation 3.1,

$$\begin{aligned} R_{ij}^2 \;=\; & r_{i_x}^2 - r_{i_x} r_{j_x} - r_{i_x} r_{j_x} + r_{j_x} r_{j_x} \\ & + r_{i_y}^2 - r_{i_y} r_{j_y} - r_{i_y} r_{j_y} + r_{j_y} r_{j_y} \\ & + r_{i_z}^2 - r_{i_z} r_{j_z} - r_{i_z} r_{j_z} + r_{j_z} r_{j_z}. \end{aligned} \tag{3.2}$$

Equation 3.2 can be linearized as

$$\begin{aligned} R_{ij}^2 \;=\; & r_{i_x}^2 - r_{i_x} r_{j_x} + (r_{j_x} - r_{i_x}) \tilde{r}_{j_x} \\ & + r_{i_y}^2 - r_{i_y} r_{j_y} + (r_{j_y} - r_{i_y}) \tilde{r}_{j_y} \\ & + r_{i_z}^2 - r_{i_z} r_{j_z} + (r_{j_z} - r_{i_z}) \tilde{r}_{j_z} \end{aligned} \tag{3.3}$$

where a valve is assumed for r_{j_x}, r_{j_y}, and r_{j_z} in order to solve for $\tilde{r}_{j_x}$, $\tilde{r}_{j_y}$, and $\tilde{r}_{j_z}$.

[1] This section was written in the early 1990's before commercial software was readily available. Commercial software will be discussed following this section.

This can be written in matrix form, for one laser, as

$$\begin{aligned} &\{ \; (r_{j_x} - r_{i_x}) \quad (r_{j_y} - r_{i_y}) \quad (r_{j_z} - r_{i_z}) \; \} \begin{pmatrix} \tilde{r}_{j_x} \\ \tilde{r}_{j_y} \\ \tilde{r}_{j_z} \end{pmatrix} \qquad (3.4) \\ &= \left(R_{ij}^2 - (r_{i_x}^2 + r_{i_y}^2 + r_{i_z}^2) + r_{i_x} r_{j_x} + r_{i_y} r_{j_y} + r_{i_z} r_{j_z} \right) \\ &= R_{ij}^2 - R_i^2 + \begin{pmatrix} r_{i_x} & r_{i_y} & r_{i_z} \end{pmatrix} \begin{pmatrix} r_{j_x} \\ r_{j_y} \\ r_{j_z} \end{pmatrix}. \qquad (3.5) \end{aligned}$$

This matrix notation can be used for three lasers. For three laser measurements, the matrices are

$$\begin{aligned} &\left\{ \begin{pmatrix} r_{j_x} & r_{j_y} & r_{j_z} \\ r_{j_x} & r_{j_y} & r_{j_z} \\ r_{j_x} & r_{j_y} & r_{j_z} \end{pmatrix} - \begin{pmatrix} r_{1_x} & r_{1_y} & r_{1_z} \\ r_{2_x} & r_{2_y} & r_{2_z} \\ r_{3_x} & r_{3_y} & r_{3_z} \end{pmatrix} \right\} \begin{pmatrix} \tilde{r}_{j_x} \\ \tilde{r}_{j_y} \\ \tilde{r}_{j_z} \end{pmatrix} = \qquad (3.6) \\ &\begin{pmatrix} R_{1j}^2 \\ R_{2j}^2 \\ R_{3j}^2 \end{pmatrix} - \begin{pmatrix} R_1^2 \\ R_2^2 \\ R_3^2 \end{pmatrix} + \begin{pmatrix} r_{1_x} & r_{1_y} & r_{1_z} \\ r_{2_x} & r_{2_y} & r_{2_z} \\ r_{3_x} & r_{3_y} & r_{3_z} \end{pmatrix} \begin{pmatrix} r_{j_x} \\ r_{j_y} \\ r_{j_z} \end{pmatrix}. \end{aligned}$$

Solving for $(\tilde{r}_{j_x}, \tilde{r}_{j_y}, \tilde{r}_{j_z})$,

$$\begin{aligned} \begin{pmatrix} \tilde{r}_{j_x} \\ \tilde{r}_{j_y} \\ \tilde{r}_{j_z} \end{pmatrix} &= \left\{ \begin{pmatrix} r_{j_x} & r_{j_y} & r_{j_z} \\ r_{j_x} & r_{j_y} & r_{j_z} \\ r_{j_x} & r_{j_y} & r_{j_z} \end{pmatrix} - \begin{pmatrix} r_{1_x} & r_{1_y} & r_{1_z} \\ r_{2_x} & r_{2_y} & r_{2_z} \\ r_{3_x} & r_{3_y} & r_{3_z} \end{pmatrix} \right\}^{-1} \qquad (3.7) \\ &\left\{ \begin{pmatrix} R_{1j}^2 \\ R_{2j}^2 \\ R_{3j}^2 \end{pmatrix} - \begin{pmatrix} R_1^2 \\ R_2^2 \\ R_3^2 \end{pmatrix} + \begin{pmatrix} r_{1_x} & r_{1_y} & r_{1_z} \\ r_{2_x} & r_{2_y} & r_{2_z} \\ r_{3_x} & r_{3_y} & r_{3_z} \end{pmatrix} \begin{pmatrix} r_{j_x} \\ r_{j_y} \\ r_{j_z} \end{pmatrix} \right\}. \end{aligned}$$

3.1.2 Multilateration

Fred Schwab worked out the algorithm using multiple measurements (> 3) in GBT Memo 37[44]. For the GBT, there will be redundant measurement paths to all retroreflectors, so this data will be used to provide a stronger network of measurements.

3.2 Commercially available software

3.2.1 STAR*NET

STAR*NET is a least squares reduction package for surveying. It is almost everything one would need to process laser rangefinder data. It is written for batch operation and does not lend itself to real-time operation, but is sufficient for post-processing data. It was a DOS program, but it has been rewritten for Windows.

3.2.2 General purpose software

Something like Mathematica could probably be adapted fairly easy.

3.2.3 National Physical Lab

The National Physical Lab (NPL) is very active in the multilateration field[45]. They have a software group, so it would behoove one to talk with them before investing in additional software. It is interesting that they assume no known baselines, i.e., plop the instruments down and bootstrap up from many multilateration poses of a target.

3.2.4 Differential Approximations

For a lot of measurements, the absolute coordinate is not necessary. For example, measuring small movements do not require absolute coordinates. Goldman derived movements of the GBT feed arm using approximate coordinates for the instruments[46].

3.2.5 Applying Constraints

In some instances, movements can be assumed to be constrained and thus the number of degrees of freedon can be reduced. For example; to first order, it is probably a good approximation that the elevation bearing weldments do not move up and down appreciably for a rotation in elevation.

3.3 Error Analysis

Fred Schwab also worked out the preliminary error analysis in GBT Memo 37[44] and in an interactive Fortran program. This needs to be refined when the final architecture starts to become fixed and the performance of the instrument is documented. The trilateration algorithm will need to include weighted measurements in order to achieve the highest accuracy.

STAR*NET does an excellent job of error analysis. It will also do the error analysis before doing the measurements in order to perform measurement scenarios before doing the actual survey. See Goldman's memo on the subreflector for an example[47].

Chapter 4

Acoustic Thermometry

One problem with applying equation 5.18 is measuring the temperature along the path of interest. It is expected that the air temperature will not be a constant through the path due to shadows, variable ground cover, changes in elevation, radiant energy reflecting from the dish, and cloud patterns. The integrated temperature along a path can be measured using acoustic thermometry[48, 49, 50, 51, 52, 53, 54]. Reference [53] develops the equations for the speed of sound in dry and moist air as a function of temperature and water vapor pressure. From equation (3.3), the speed of sound in dry air is

$$c_d = \sqrt{\frac{\gamma RT}{M}} \tag{4.1}$$

where

$$\begin{aligned} \gamma &= \text{specific heat ratio} \\ &= 1.402 \\ R &= \text{gas constant} \\ &= 8.314 \text{ (joule/mole °K)} \\ T &= \text{temperature (°K)} \\ M &= 28.980 \times 10^{-3} \text{(kg/mole)}, \end{aligned}$$

or,

$$c_d = 20.0553 \sqrt{T} \text{ (m/s)}. \tag{4.2}$$

Notice that the speed of sound for dry air is not a function of pressure. The speed of sound for dry air at 20 °C is 343.379 m/s.

From equation (3.2) of reference [53], the speed of sound in humid atmosphere is,

$$c_h = c_d \left[1 - \frac{P_w}{P} \left(\frac{\gamma_w}{\gamma_a} - \frac{5}{8} \right) \right]^{-1/2} \tag{4.3}$$

where

$$\begin{aligned} c_d &= \text{speed of sound in dry air (m/s)} \\ c_h &= \text{speed of sound in humid air (m/s)} \\ P &= \text{total atmospheric pressure (mb)} \\ P_w &= \text{partial water vapor pressure (mb)} \\ \gamma_w &= \text{ratio of specific heats for water} \\ &= 1.004 \end{aligned}$$

$$\begin{aligned} \gamma_a &= \text{ratio of specific heats for air} \\ &= 1.402 \end{aligned}$$

or,

$$c_h = 20.0553\sqrt{T}\left(1 - 0.091119\frac{P_w}{P}\right).^{-1/2} \tag{4.4}$$

The propagation time, Δt, for an acoustic wave to travel a distance s is,

$$\Delta t = \frac{s}{20.0553\sqrt{T}}\left(1 - 0.091119\frac{P_w}{P}\right).^{1/2} \tag{4.5}$$

The temperature, T, can be measured experimentally by measuring s, Δt, P, and P_w where,

$$T = \left(1 - 0.091119\frac{P_w}{P}\right)\left(\frac{c_h}{20.0553}\right)^2 \tag{4.6}$$

or,

$$T = \left(1 - 0.091119\frac{P_w}{P}\right)\left(\frac{s}{20.0553\Delta t}\right).^2 \tag{4.7}$$

The integrated path value of T from an acoustic thermometry experiment can then be used to calculate the density factors, D_s and D_w.

4.0.1 Sensitivity of the Speed of Sound

At 20 °C, 933 mb, and 50% relative humidity;

$$c_h = 343.577 \text{ m/s} \tag{4.8}$$

$$\frac{\partial c_h}{\partial T} = 0.598\,212 \text{ m/s/°C} \tag{4.9}$$

$$\frac{\partial c_h}{\partial P} = -0.000\,210 \text{ m/s/mb} \tag{4.10}$$

$$\frac{\partial c_h}{\partial h} = 0.003\,941 \text{ m/s/\%rh} \tag{4.11}$$

$$\frac{\partial c_h}{\partial P_w} = 0.016\,796 \text{ m/s/mb} \tag{4.12}$$

$$\Delta t = 2.910\,55 \times 10^{-3} \text{ s/m} \tag{4.13}$$

$$\frac{\partial \Delta t}{\partial T} = -5.067 \times 10^{-6} \text{ s/m/°C}. \tag{4.14}$$

Notice that the temperature sensitivity is very high. However, for a single path instrument 1.3 mph/degree is lost in the wind speed. A series of simple experiments was conducted using an autocorrelation technique [52] to measure the delay. Delays were automatically measured using a PC, an A/D board, arbritary function generator, audio amplifier, and a parabolic microphone. It is felt that an array or dual path architecture can be used for the GBT, but work has been halted in this area due to manpower limitations.

```
eq33=(gamma r tk/m)^(1/2)
gamma=1.402
r=8.314
m=28.980 10^(-3)
speed=eq33(1-pw/p(gammaw/gammaa-5/8))^(-1/2)
gammaw=1.004
gammaa=1.402ch[p_,t_,h_]=speed
dchdt[p_,t_,h_]=N[D[speed,t],10]
dchdh[p_,t_,h_]=N[D[speed,h],10]
dchdp[p_,t_,h_]=N[D[speed,p],10]

dtimedt[p_,t_,h_]=N[D[time,t],10]
temp[p_,t_,h_,time_]=(1-.091119 pw/p)(s/(20.0553 time))^2
```

Figure 4.1: Mathematica Program SOUND.EQ

Chapter 5

Signal Processing

Digital signal processing to extract the phase of the reflected signal greatly enhances the system over previous analog EDMs[24, 55, 56, 43, 57, 58, 59, 60, 61, 62, 63, 64, 65].

5.1 Laser Modulation and Detection

5.1.1 Frequency Synthesis

The laser diode is directly amplitude modulated at 1500.000 MHz. The detected signal is amplified and mixed with a phase locked (1500.000 MHz + IF) source, where the IF is typically 1 kHz, but can run up to 10 kHz. The 1500.000 MHz and 1500.000 MHz + IF signals are derived from a 100.000 Mhz reference and a TTL IF from the computer control system. The 100.000 MHz reference is multiplied times 15 to produce 1500.000 Mhz. The 1500.000 MHz signal is then phase locked to the TTL IF to produce the offset. Two models of oscillators are used. The NRAO unit designed by John Payne is shown on drawing A35402K002. The production oscillators were designed by Magnum Microwave Corporation and are shown on drawing D35420????.

Maser Phase Noise

Initial trials using a maser 100.000 MHz reference revealed a 57 Hz phase noise problem. (Insert section by John Payne on references)

Rubidium Oscillator

A Rubidium oscillator reference was chosen. The phase noise and stability are ??? The distribution circuit is shown on drawing D35420??? .

5.1.2 Laser Circuit

Two laser models were built by Richard Bradley. The first unit is shown on drawing D35420????. The production unit is shown on drawing D35420S004.

5.1.3 Detector Circuit

The detector is a PIN diode. The detected signal is amplified and mixed with 1500.000 MHz to produce the IF. Two models of detectors were used. The experimental units are shown on drawing D35420??? and the production units are shown on drawing D35420S???.

5.2 Measurement of Phase

There are a number of ways to measure the phase of two signals. One can measure the time difference between the zero crossings of the two signals. The Clark-Hess model 6000 measures the time difference between the front and back zero crossings and takes the average. This has the advantage of working for any frequency, but is sensitive to noise around the zero crossing. It is also sensitive to waveform distortion due to shifts in the average signal value of the waveform produced by ac coupling. For example, if the signal is clipped on the top; the signal average, or zero level, drops down below the unclipped value. This causes the comparitor trigger to shift and thus a phase shift.

Where the frequency is known, a digital synchronous detection method can be used. This is the technique now used for digital lock-in amplifiers. Stanford Research explains the merits very well in a report[66]. This method is relatively immune to noise at frequencies below the Nyquist rate, but also suffers from the same waveform distortion problem. Of course, the higher harmonic content introduced by distortion can be detected by modifying equations 5.1 and 5.2.

A 16 bit analog to digital converter is used to sample the 1 kHz signal into a sequence of samples s_j. Timing for the A/D conversions is precisely controlled using an 8253 counter/timer chip. The 8253 generates n sample trigger pulses to the A/D board for each 1 kHz square wave cycle. The 1 kHz square wave is derived from the n pulses, thus insuring exact phase synchronization. A gate signal to initiate the A/D conversions is also generated by the 8253. This is illustrated in Creager's talk[67]. Knowing the exact phase relationship of the sampled data to the reference signal allows one to compute the phase of the fundamental harmonic very simply. For a signal sampled over m complete cycles, there is no *leakage* or windowing problems with a discrete Fourier series calculation. For retroreflector i, the Fourier cosine and sine components are

$$a_i = \sum_{j=0}^{mn-1} s_j \cos(\frac{2\pi j}{n}) \tag{5.1}$$

$$b_i = \sum_{j=0}^{mn-1} s_j \sin(\frac{2\pi j}{n}). \tag{5.2}$$

Where
n = number of samples per cycle
m = number of cycles sampled.

The signal amplitude and phase are

$$A_i = \frac{2}{mn}(a_i^2 + b_i^2)^{1/2} \tag{5.3}$$

$$\phi_i = \tan^{-1}(\frac{b_i}{a_i}). \tag{5.4}$$

In order to minimize the number of floating point operations and thus minimize computing time, equations 5.1 and 5.2 can be cast into the form

$$a_i = \sum_{l=0}^{n-1}\Big(\cos(2\pi l/n)\sum_{k=0}^{m-1} s_{nk+l}\Big) \tag{5.5}$$

$$b_i = \sum_{l=0}^{n-1}\Big(\sin(2\pi l/n)\sum_{k=0}^{m-1} s_{nk+l}\Big). \tag{5.6}$$

The inner sum is performed using integer arithmetic, and of course needs to be calculated only once for each l.

5.2.1 Phase Noise

Using the digital method; harmonic, as well as high frequency, noise will be rejected. There will be a significant error introduced by fundamental frequency noise however. For example; stray laser reflections, multiple retroreflector reflections, and electronic crosstalk will contribute to an additional fundamental component. The extreme case would be when the noise is in quadrature with the signal. In that case, the phase error is

$$\phi_\sigma = \tan^{-1}\Big(\frac{\text{noise}}{\text{signal}}\Big). \tag{5.7}$$

The distance error would be

$$D_\sigma = \tan^{-1}\Big(\frac{\text{noise}}{\text{signal}}\Big)\frac{\lambda_a}{4\pi}. \tag{5.8}$$

For example; with a quadrature signal-to-noise ratio of 1000:1 at a 1.5 GHz modulation frequency, the maximum distance error would be 15.9 μm.

5.3 Phase as a Function of Distance

For EDM, the problem is how to convert measured phase into distance. Starting with the asumption that with the electronics used for the instruments (LO=1500.001 MHz instead of 1499.999 MHz), the measured phase decreases for an increase in distance (which was empirically determined), i.e.,

$$\partial\phi/\partial D = -2\pi/\lambda_a/2, \tag{5.9}$$

we can write

$$d_l + 2D_i + d_d = n_i\lambda_a - \frac{\phi_i}{2\pi}\lambda_a - \frac{\phi_e}{2\pi}\lambda_e, \tag{5.10}$$

where
d_l =distance from laser to mirror
d_d =distance from mirror to detector
D_i =distance from mirror to retroreflector i
n_i =number of integer wave lengths over total path to retroreflector i
ϕ_i =measured phase for retroreflector i
ϕ_e =total electronic phase shift
λ_a =atmospheric group wave length
λ_e =electrical group wave length.

It is assumed that the mirror rotates about the intersection of the azimuth and elevation axes, and the laser beam intersects the mirror at the same point. If this is not the case, d_l, d_d, and D_i will depend on the azimuth and elevation angles. From equation 5.10, the measured phase for retroreflector i is

$$\phi_i = -\frac{2\pi}{\lambda_a}[(d_l + d_d + \frac{\phi_e}{2\pi}\lambda_e) + (2D_i - n_i\lambda_a)]. \tag{5.11}$$

5.4 Removal of Electronic Drift

Low frequency drifts in ϕ_e, as well as d_l and d_d, can be removed by referencing to a fixed cube at a distance D_0 from the mirror. From equation 5.11,

$$\phi_i - \phi_0 = -\frac{2\pi}{\lambda_a}[2(D_i - D_0) - (n_i - n_0)\lambda_a]. \tag{5.12}$$

Let

$$\tilde{\phi}_i = \text{Mod}\{\phi_i - \phi_0, 2\pi\}, \tag{5.13}$$

i.e., $0 \leq \tilde{\phi}_i < 2\pi$.

$$\tilde{\phi}_i = -\frac{4\pi}{\lambda_a}(D_i - D_0) - 2\pi(n_i - n_0) \tag{5.14}$$

or

$$D_i = (2\pi(n_i - n_0) - \tilde{\phi}_i)\frac{\lambda_a}{4\pi} + D_0 \tag{5.15}$$

5.5 Corrections for Group Refractive Index

The wavelength in air, λ_a, is a function of temperature, humidity, and pressure. This can be expressed as a function of the group refractive index as,

$$\lambda_a = \frac{c}{n_g f}. \tag{5.16}$$

Substituting into equation 5.14,

$$\tilde{\phi}_i = -\frac{4\pi n_g f}{c}(D_i - D_0) - 2\pi(n_i - n_0) \tag{5.17}$$

or,

$$D_i = \frac{c}{2n_g f}\left(n_i - n_0 - \frac{\tilde{\phi}_i}{2\pi}\right) + D_0. \tag{5.18}$$

Methods for measuring the group refractive index are discussed in [25].

5.6 Corrections for retroreflector glass

The derivation above assumes a hollow retroreflector, but as has already been shown, a glass retroreflector has an additional correction due to the increased group refractive index of glass, i.e., the time delay through the glass is longer, and thus the measured phase of a glass retroreflector would be less that a hollow retroreflector. By convention, we decided to assign a glass correction factor to the retroreflectors such that

$$D_i = \frac{c}{2n_g f}\left(n_i - n_0 - \frac{\tilde{\phi}_i}{2\pi} - \frac{\phi_{ic}}{2\pi}\right) + D_0. \tag{5.19}$$

where ϕ_{ic} is the glass calibration offset. An example caclulation is included in the GBT Archive file[68].

5.7 Additional references

Additional references that may be of interest include[44, 3, 46, 69, 70, 71, 72, 73].

Chapter 6

Optics and Mirror System

This section is incomplete, but the outline is included. Additional references include[74, 75, 76, 77, 78, 79, 80, 81, 82, 83, 79, 84, 85, 86]

There are some real subtleties to watch out for in the optics. Time does not permit a proper expansion on the subject, but I will possibly write a stand-alone article later. In general the problems are:

1. The group index of refraction produces a spherical aberation of the group at the focal point, i.e., the phase of the group for the rays through the outer edge of the lens are retarded more that the rays through the center. In retrospect, we should have used reflective optics.
2. The finite size of the detector introduces a phase shift, depending on where the image falls. This is helped by using short focal length optics. A better solution would be to use a beam splitter and quadrant detector to servo the image to a fixes spot on the detector.
3. Since the detector falls at the focal point of the optics, scatter reflects back through the optics– like a cat's eye reflector. Care must be taken to avoid multiple path reflections.
4. Care must be taken to avoid reflections back into the laser, which can introduce a phase shift through the power regulation feedback circuit in the laser.
5. Extreme care must be taken to ensure the electronics is not sensitive to amplitude, e.g., non-linear capacitors.
6. AR coatings are a must. Gold is too soft to clean, silver tarnishes, and aluminum is inefficient at 780 nm.

6.1 Laser Safety

[87, 88, 89, 90, 91]

6.2 Optics

[92, 93, 94, 95]

6.2.1 Laser

[?, 96, ?]

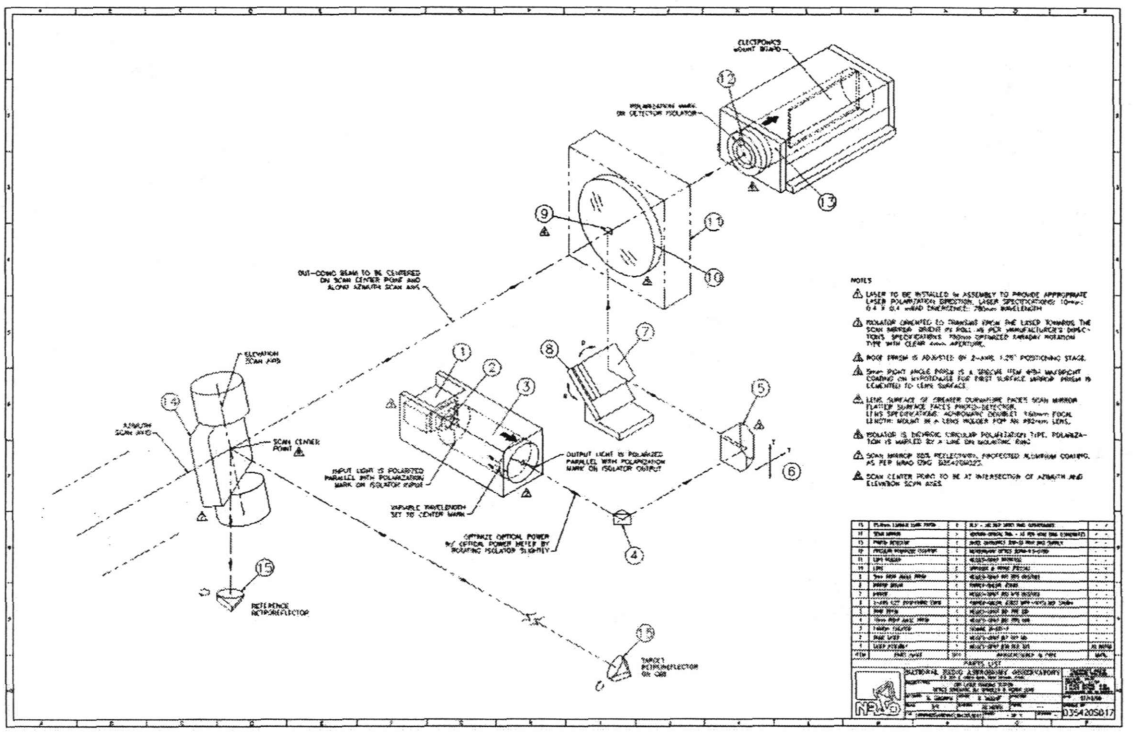

Figure 6.1: PSH97 Optics train.

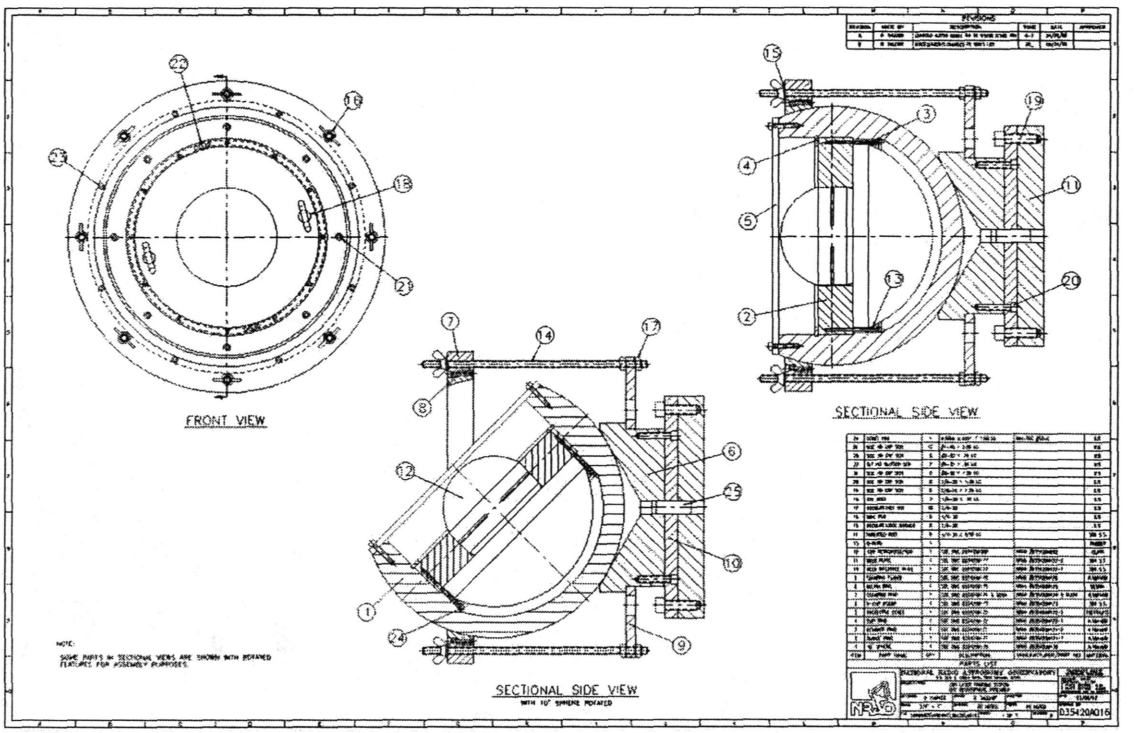

Figure 6.2: Spherical retroreflector.

6.2.2 Mirror Coatings

Gold

Aluminum

Thin Film

6.2.3 Detector

[97]

Optical Isolators

6.2.4 Retroreflectors

[98, 99, 100, 101, 102, 103, 104, 105, 106, 107, 108, 109, 110]

6.2.5 Polarization

6.2.6 Gaussian Bean Analysis

laser

coated mirrors

retroreflectors

isolator

6.3 Servo Mirror

6.3.1 Servo Motors

6.3.2 Replicated Mirror

6.3.3 Mounting Base

6.4 Control System

6.4.1 Computer Board

6.4.2 A/D board

6.4.3 Servo Control

[111, 112]

6.4.4 Servo Amplifiers

6.4.5 Ethernet Board

6.4.6 RFI Design Factors

[113, 114]

6.5 Alignment

[33, 115]

Chapter 7

Calibration

[116, 117, 115, 118, 119, 30, 120, 121, 122, 123, 33, 43, 124, 28, 7, 110, 38, 125, 126, 127, 8, 128, 61, 62, 129, 130, 131, 132, 133, 34, 103, 104, 105, 106, 98, 99, 100, 101, 107, 108, 109, 134, 135, 136, 137, 138, 139, 140, 80, 36, 37, 141, 142, 143, 144, 29, 35, 145, 146, 32]

7.1 Laser Mirrors

7.1.1 Mirror Adjustments

7.1.2 Laser Adjustments

7.1.3 Detector Focus

7.1.4 Encoders

7.1.5 Mounting Plate

7.1.6 Reference Cube

7.2 Monuments

7.2.1 Coordinate

7.2.2 True North Orientation

7.2.3 Mount Pointing

7.2.4 Elevation

Pellissier H5 Level

Description

Proceedure

Instrument Constant

7.3 Length

7.3.1 HP Laser Interferometer

7.3.2 Gage Blocks

7.3.3 Invar Wire

7.3.4 Topcon Total Station

7.4 Retroreflector Offset

7.5 Linearity

Chapter 8

Experimental Data

[147, 148, 149]

- Refractivity
  1. typical acquired data (D0309_1)
  2. typical processed data (D0309_1)
  3. refractometer calibration
- Oscillator
  1. Magnum oscillator phase noise vs cycles (08/15/94 ZRG)
  2. Magnum oscillator-log log (08/15/94)
  3. A/D system timing diagram
- Linearity
  1. ranger vs interferometer (DL0504_1)
  2. linearity residual vs interferometer (DL0504_1)
- Retroreflectors
  1. reflected power vs angle
  2. amplitude vs angls (D0411_1)
  3. azimuth scan
  4. elevation scan
  5. rotation
- Acoustic Thermometry
  1. signature wave (1-13-93)
  2. signal data (1-20-93)
  3. cross-correlation data (1-20-93)

Chapter 9

GBT Architecture

[150, 151, 44, 152, 153, 59, 154, 155, 156, 157, 158, 159, 5, 160, 161]

9.0.1 Ground Instruments

9.0.2 GBT Moving Instruments

9.0.3 Survey and Calibration

9.0.4 Tracking Model

Chapter 10

Software

[156, 162, 163, 159, 164, 165, 166, 167, 168, 169, 170, 171, 6] [161, 172, 173, 174, 41, 175, 42, 176, 177, 178, 179, 180, 181] [182, 183, 81, 69, 184, 169, 171, 160, 173, 41]

10.1 Architecture

10.2 Algorithms

Chapter 11

Panel Setting Instrument

[185, 186, 187, 145]

11.1 Statement of Problem

11.2 Description of Instrument

11.3 Equations

11.4 Integration With RSI CMM Data and Best Fit

11.5 Operation

Bibliography

[1] David H. Parker. The Green Bank Telescope laser metrology R&D project, a review and bibliography. GBT Memo 166, the National Radio Astronomy Observatory, 1997.

[2] David H. Parker. The GBT laser metrology R&D project, a review and bibliography. Technical Report L0294, the National Radio Astronomy Observatory, 1997.

[3] D. E. Hogg. Atmospheric limitations on the gbt laser ranging system. Technical Report 45, GBT Memo Series, 1990.

[4] Dr. Sebastion von Hoerner. Remarks about dynamics, atmoshere and summaries. Technical Report 56, GBT Memo Series, 1990.

[5] Leonid Kogan. A study of the effect of vertical stratification of the atmosphere on the performance of the gbt. Technical Report 97, GBT Memo Series, 1993.

[6] Ronald J. Maddalena. Refraction, weathe station components, and other details for pointing the gbt. Technical Report 112, GBT Memo Series, 1994.

[7] Robert J. List. *Smithsonian Meteorological Tables.* Smithsonian International Press, sixth edition, 1971.

[8] US Department of Commerce and Weather Bureau. *Manual of Barometry.* US govt, first edition, 1963.

[9] J. Beers and T. Doiron. Verification of revised water vapour correction to the index of refraction of air. *Metrologia*, 29:315–316, 1992.

[10] Erik Bergstrand. A preliminary determination of the velocity of light. *Arkiv for Matematik, Astronomi o. Fysik*, 36A(20):1–11, February 1949.

[11] Erik Bergstrand. Determination of the velocity of light. *Handbuch der Physik*, 24:1–4.

[12] Erik Bergstrand. A check determination of the velocity of light. *Arkiv for Fysik*, 3(26):479–490, February 1951.

[13] K. P. Birch and M. J. Downs. The results of a comparison between calculated and measured values of the refractive index of air. *J. Phys. E:*, 21:694–695, 1988.

[14] M. Mark Colavita, Michael Shao, and David H. Staelin. Two-color method for optical astrometry: theory and preliminary measurements with the mark iii stellar interferometer. *Applied Optics*, 26(19):4113–4122, October 1987.

[15] M. Mark Colavita, Michael Shao, and David H. Staelin. Atmospheric phase measurements with the mark iii stellar inerferometer. *Applied Optics*, 26(19):4106–4112, October 1987.

[16] K. B. Earnshaw and E. Norman Hernandez. Two-laser optical distance-measuring instrument that corrects for the atmospheric index of refraction. *Applied Optics*, 11(4):749–754, April.

[17] Bengt Edlen. The refractive index of air. *Metrologia*, 2(2):71–80, 1966.

[18] C. S. Gardner. Effects of random path fluctuation on the accuracy of laser ranging systems. *Applied Optics*, 15(10):2539–2545, October.

[19] Frank E. Jones. The refractivity of air. *Journal of Research*, 86(1):27–32, January-February 19880.

[20] Paul K. Manhart. Two-wavelength optical-path-difference mapping. Technical report, NASA, November 1990.

[21] Hirokazu Matsumoto and Tokuyuki Honda. High-accuracy length-measuring interferometer using the two-colour method of compensating for the refractive index of air. *Meas. Sci. Technol.*, 3:1084–1086, 1992.

[22] James C. Owens. Optical refractive index of air: Dependence on pressure, temperature and composition. *Applied Optics*, 6(1):51–59, January 1967.

[23] Dr. Gunter Wilkening. The measurement of the refractive index of the air. *IMEKO Symposium on Laser Applications in Precision Measurement*, pages 17–25, 1986.

[24] J.M.Rueger. *Electronic Distance Measurement.* Springer-Verlag, third edition, 1990.

[25] David H. Parker. Methods for correcting the group index of refraction at the ppm level for outdoor electronic distance measurement. In *Proceedings ASPE 2001 Annual Meeting*, pages 86–87. American Society for Precision Engineering, 2001.

[26] Ronald N. Bracewell. *The Fourier Transform and its Applications.* McGraw-Hill Book Company, second edition, 1986.

[27] Princo Instruments, Inc. *Instruction Booklet for use with Princo Fortin Type Mercury Barometers.*

[28] S. Letestu, editor. *International Meteorological Tables.* sec. of the WMO, 1966.

[29] David H. Parker, Bill Radcliff, and John Shelton. Green bank site survey information. GBT Memo 223, the National Radio Astronomy Observatory, 2004.

[30] Herbert Goldstein. *Classical Mechanics.* Addison-Wesley, 1980.

[31] Harold Jeffreys and Bertha Swirles Jeffreys. *Methods of Mathematical Physics.* Cambridge University Press, second edition, 1950.

[32] David H. Parker and John Shelton. Calibration of kelvin clamp euler angles for absolute instrument orientation. GBT Memo 229, the National Radio Astronomy Observatory, 2004.

[33] Philip Kissam. *Optical Tooling for Precise Manufacturing and Alignment.* McGraw–Hill, 1962.

[34] U.S. Department of Commerce. Plane coordinate projection tables, west virginia. Technical Report 275, Coast and Geodetic Survey, 1952.

[35] David H. Parker, Bill Radcliff, and John Shelton. Nrao green bank metrology lab capabilities facilities and resources. GBT Memo 224, the National Radio Astronomy Observatory, 2004.

[36] John Shelton. The GBT metrology system–ZP calibration procedure. Technical Report L0460, the National Radio Astronomy Observatory, 1998.

[37] David H. Parker. Laser calibration lab record book #4. Technical Report L0731, the National Radio Astronomy Observatory, 1999.

[38] Richard L. Elgin. *1994 Celestial Observation Handbook and Ephemeris.* Elgin, Knowles & Senne, 1993.

[39] Russell C. Brinker and Roy Minnick, editors. *The Surveying Handbook.* Chapman & Hall, second edition, 1995.

[40] John C. Polasek. Matrix analysis of gimbaled mirror and prism systems. *Journal of the Optical Society of America*, 57(10):1193–1201, 1967.

[41] Donald C. Wells and L. King. The GBT tipping-structure model in c. Technical Report 124, GBT Memo Series, 1995.

[42] Grace Buzanoski. Gbt finite element analysis macros in quattro pro. Technical Report 130, GBT Memo Series, 1995.

[43] Simo H. Laurila. *Electronic Surveying In Practice.* John Wiley & Sons, 1983.

[44] Frederic R. Schwab. Error sensitivity of gbt laser metrology. Technical Report 37, GBT Memo Series, 1990.

[45] E. B. Hughes, A. Wilson, and G. N. Peggs. Design of a high-accuracy CMM based on multilateration techniques. *Ann. CIRP*, 49(1):391–394, 2000.

[46] Michael Goldman. Differential measurements of GBT tipping structure retroreflector vibrational motions. Technical Report L0543, the National Radio Astronomy Observatory, 1999.

[47] Michael Goldman. A summary of STAR*NET simulations of subreflector position measurements using the GBT laser metrology system. Technical Report A0118, the National Radio Astronomy Observatory, 1998.

[48] M. W. Dadd. Acoustic thermometry in gases using pulse techniques. *High Temperature Technology*, 1(6):333–342, November 1983.

[49] Glenis Moore. Acoustic thermometry, a sound way to measure temperature. *Electronics & Power*, pages 675–677, September 1984.

[50] Glen Ballou, editor. *Handbook for Sound Engineers, The New Audio Cyclopedia.* Howard W. Sams, second edition, 1991.

[51] Don Davis and Carolyn Davis. *Sound System Engineering*, chapter 7. Howard W. Sams, second edition, 1987.

[52] Julius S. Bendat and Allan G. Piersol. *Engineering Applications of Correlation and Spectral Analysis.* Wiley, 1980.

[53] J. A. Kleppe. *Engineering Applications of Acoustics.* Artech House, first edition, 1989.

[54] David H. Parker, John M. Payne, S. A. Massey, and S. L. Riley. The feasibility of acoustic thermometry for laser edm temperature correction. Technical Report 79, GBT Memo Series, 1992.

[55] C. D. Burnside. *Electronic Distance Measurement.* BSP Professional Books, third edition, 1991.

[56] T. Kemeny and K. Havrilla, editors. *Laser Applications in Precision Measurement.* Nova Science Publishers, first edition, 1987.

[57] John M. Payne. An optical distance measuring instrument. *The Review of Scientific Instruments*, 44(3):304–306, March 1973.

[58] J.M. Payne, D. Parker, and R.F. Bradley. Rangefinder with fast multiple range capability. *Rev. Sci. Instrum.*, pages 3311–3316, June 1992.

[59] John M. Payne and David H. Parker. The laser ranging system for the gbt. Technical Report 57, GBT Memo Series, 1990.

[60] David C. Williams and Jason E. Banyard. Comparison of long-range and interferometric laser distance instruments using multiple reflections. In *Laser Dimensional Metrology: Recent Advances for Industrial Application, SPIE Proceedings Volume 2088*, pages 46–54. SPIE, 1993.

[61] Larry D. Hothem and Charles J. Fronczek. Report on test and demonstration of macrometer model v-1000 interferometric surveyor. Technical Report FGCC-IS-83-2, Federal Geodetic Control Committee, Instrument Subcommittee, 1983.

[62] Stephen R. DeLoach. Test and evaluation of total station instruments. Technical Report FGCC-IS-87-1, Federal Geodetic Control Committee, Instrument Subcommittee, 1987.

[63] K. D. Froome. Precision distance measurement based on the velocity of light. *Sci. Prog., Oxf.*, 59:199–223, 1971.

[64] K. S. Hashemi, P. T. Hurst, and J. N. Oliver. Sources of error in a laser rangefinder. *Rev. Sci. Instrum.*, 65(10):3165–3171, October 1994.

[65] A. D. Nizhenskii and et al. Phase-type laser range finder. *Measurement Techniques*, 27(2):127–129, February 1984.

[66] Stanford Research. Lock-in amps go digital. Technical Report L0180, the National Radio Astronomy Observatory, 1991.

[67] Ray Creager. The green bank telescope laser metrology software. Technical Report L0802, the National Radio Astronomy Observatory.

[68] David H. Parker. Example calculations of rangefinder coordinates and distances. Technical Report L0699, the National Radio Astronomy Observatory, 2002.

[69] David H. Parker. Notes on 8254 timing. Technical Report L0337, the National Radio Astronomy Observatory, 1997.

[70] David H. Parker. Letter to kevan hashemi. Technical Report L0276, the National Radio Astronomy Observatory, 1994.

[71] Kevan Hashemi. Rev sci inst article. Technical Report L0737, the National Radio Astronomy Observatory, 1994.

[72] Kevan Hashemi. Sources of error in a laser rangefinder. Technical Report L0166, the National Radio Astronomy Observatory, 1994.

[73] Mark Leach. Laser diode modulation depth). Technical Report L0102, the National Radio Astronomy Observatory, 1995.

[74] David H. Parker. The gbt laser metrology system optics design experiments. Technical Report L0070, the National Radio Astronomy Observatory, 1995.

[75] Michael Goldman. Expected gaussian beam spreading of the melles-griot LT0021MD. Technical Report L0170, the National Radio Astronomy Observatory, 1996.

[76] Michael Goldman. Waist to waist imaging. Technical Report L0214, the National Radio Astronomy Observatory, 1996.

[77] David Bradley. Measurements of the GBT ball-retroreflector visible aperture. Technical Report L0082, the National Radio Astronomy Observatory, 1996.

[78] David Bradley. 10 mw laser power vs distance from source. Technical Report L0097, the National Radio Astronomy Observatory, 1996.

[79] John Payne and Rich Bradley. Laser detector design notes. Technical Report L0378, the National Radio Astronomy Observatory, 1997.

[80] John Shelton. Mechanical measurements of spherical retroreflectors. Technical Report L0156, the National Radio Astronomy Observatory, 1997.

[81] Gaddy. How to write a pid algorithm. Technical Report L0312, the National Radio Astronomy Observatory, 1997.

[82] John Payne. Laser rangefinder design notes. Technical Report L0660, the National Radio Astronomy Observatory, 1990.

[83] John Shelton. Laser ranging system mirror assembly. Technical Report L0100, the National Radio Astronomy Observatory, 1996.

[84] M. A. Goldman. Optical ray trace computations for the laser ranging system detector lense. GBT Memo 146, the National Radio Astronomy Observatory, 1996.

[85] M. A. Goldman. Ball retroreflector optics. GBT Memo 148, the National Radio Astronomy Observatory, 1996.

[86] M. A. Goldman. Laser rangefinder intensity and safety. GBT Memo 156, the National Radio Astronomy Observatory, 1996.

[87] Martin J. Valente. Laser safety. Technical Report 91, GBT Memo Series, 1992.

[88] American Conference of Governmental Industrial Hygienists. *Threshold Limit Values and Biological Exposure Indices for 1987-1988*, 1987.

[89] Pamela Georgopoulos. Laser irradiation and eye protection. *EMC Test and Design*, pages 32–34, February 1993.

[90] The Laser Institute of America. American national standard for the safe use of lasers. Technical Report ANSIZ136.1-1986, American National Standards Institute, Inc., 1986.

[91] Larryl Matthews and Gabe Garcia. *Laser and Eye Safety in the Laboratory.* IEEE Press, 1995.

[92] Max Born and Emil Wolf. *Principles of Optics.* Pergamon Press, sixth edition, 1980.

[93] Francis A. Jenkins and Harvey E. White. *Fundamentals of Optics.* McGraw–Hill, 1957.

[94] Paul A. Tipler. *Physics For Scientists and Engineers.* Worth, third edition, 1991.

[95] Douglas S. Goodman. *Bibliography of Classical Optics.* IBM Thomas J. Watson Research Center, 1985.

[96] A. E. Siegman. *An Introduction to Lasers and Masers.* McGraw-Hill Book Company, first edition, 1971.

[97] David Livigni and Xiaoyu Li. Spatial uniformity of optical detector responsivity. *Measurement Science Conference*, pages 3–13, 1992.

[98] V. V. Korotaev and E. D. Pankov. Polarization properties of corner reflectors. *The Optical Society of america*, 48(1):9–13, January 1981.

[99] Edson R. Peck. Polarization properties of corner reflectors and cavities. *Journal of the Optical Society of America*, 52(3):253–257, March 1962.

[100] Edson R. Peck. Theory of the corner-cube interferometer. *Journal of the Optical Society of America*, 38(12):1015–1024, December 1948.

[101] M. A. Player. Polarization properties of a cube-corner reflector. *Journal of Modern Optics*, 35(11):1813–1820, 1988.

[102] Edward Collett. *Polarized Light.* Marcel Dekker, 1993.

[103] H. D. Eckhardt. Simple model of corner reflector phenomena. *Applied Optics*, 10(7):1559–1566, July 1971.

[104] IMEKO. *Spherical Retroreflector for Interferometric Measurement.* Nova Science Publishers, November 1986.

[105] D. C. Hogg. Optical center of a glass corner cube: Its measurement. *Applied Optics*, 15(2):304–305, February 1976.

[106] L. A. Kivioja. The EDM corner reflector constant is not constant. *Surveying and Mapping*, pages 143–155, June 1978.

[107] J. J. Snyder. Paraxial ray analysis of a cat's-eye retroreflector. *Applied Optics*, 14(8):1825–1828, August 1975.

[108] James L. Zurasky. Cube corner retroreflector test and analysis. *Applied Optics*, 15(2):445–452, February 1976.

[109] Stephen R. Wilk. How retroreflectors really work. *Optics and Photonics News*, pages 6–7, December 1993.

[110] Daniel Malacara, editor. *Optical Shop Testing.* Wiley, 1978.

[111] Technology 80 Inc. *Inside the PID Loop - How it Works*, 1991.

[112] P. E. Wellstead and M. B. Zarrop. *Self-Tuning Systems: Control Signal Processing.* John Wiley and Sons Ltd., 1991.

[113] Ralph Morrison. *Grounding and Shielding Techniques in Instrumentation.* Wiley, 1986.

[114] Ralph Morrison and Warren H. Lewis. *Grounding and Shielding in Facilities.* Wiley, 1990.

[115] B. Austin Barry. *Construction Measurements.* Wiley, second edition, 1988.

[116] P. Pellissier. Pellissier model h5 - portable hydrostatic level/tiltmeter. Technical Report 116, GBT Memo Series, 1994.

[117] P. Pellissier. Benchmarks for accurate leveling. Technical Report 117, GBT Memo Series, 1994.

[118] Philip R. Bevington. *Data Reduction and Error Analysis for the Physical Sciences.* McGraw–Hill, 1969.

[119] Ted Busch. *Fundamentals of Dimensional Metrology.* Delmar, 1988.

[120] Bernard Hofmann-Wellenof, Herbert Lictenegger, and James Collins. *Global Positioning System.* Springer-Verlag, second edition, 1992.

[121] Barry E. Jones. *Instrument Science and Technology*, volume 1. Adam Hilger, 1982.

[122] Barry E. Jones. *Instrument Science and Technology*, volume 2. Adam Hilger, 1983.

[123] Barry E. Jones. *Instrument Science and Technology*, volume 3. Adam Hilger, 1985.

[124] Alfred Leick. *GPS Sattelite Surveying.* Wiley, first edition, 1990.

[125] P. H. Sydenham. *A Working List of Books Published on Measurement Science.* Delft University of Technology, Department of Applied Physics, 1980.

[126] P. H. Sydenham. *Handbook of Measurement Science*, volume 1. Wiley, 1982.

[127] P. H. Sydenham. *Handbook of Measurement Science*, volume 2. Wiley, 1983.

[128] Captain F. R. Gossett. Manual of geodetic triangulation. Technical Report Special Publication No. 247, Coast and Geodetic Survey, 1989.

[129] Larry D. Hothem. Geometric geodetic accuracy standards and specifications for using gps relative positioning techniques. Technical Report Version 5.0, Federal Geodetic Control Committee, 1988.

[130] Larry D. Hothem. Test and demonstration of gps satellite survey systems. Technical Report FGCC-IS-90-1, Federal Geodetic Control Committee, Instrument Subcommittee, 1990.

[131] Larry D. Hothem. Test and demonstration of three dual-frequency (l1/l2) gps satellite survey systems. Technical Report FGCC-IS-90-2, Federal Geodetic Control Committee, Instrument Subcommittee, 1990.

[132] Lt. Richard P. Floyd. Geodetic bench marks. Technical Report NOS NGS 1, National Oceanic and Atmospheric Administration, 1978.

[133] Joe D. Simmons. NIST calibration services users guide 1991. Technical Report Special Publication 250, National Institute of Standards and Technology, 1991.

[134] David H. Parker. Laser field testing record book #1 (1/15/91-2/01/94. Technical Report L0181, the National Radio Astronomy Observatory, 1994.

[135] David H. Parker. Jansky lab record book (12/13/91-3/19/97). Technical Report L0188, the National Radio Astronomy Observatory, 1997.

[136] John Findlay. Leveling the GBT azimuth track. Technical Report L0203, the National Radio Astronomy Observatory, 1992.

[137] David H. Parke. Laser calibration lab record book #1 (5/12/93-2/01/95. Technical Report L0186, the National Radio Astronomy Observatory, 1995.

[138] David H. Parker. Laser field testing record book #2 (2/10/94-3/17/97. Technical Report L0182, the National Radio Astronomy Observatory, 1997.

[139] David H. Parker, John Shelton, and Bill Radcliff. Surveying field book #1 (4/8/94-9/4/96. Technical Report L0190, the National Radio Astronomy Observatory, 1996.

[140] David H. Parker. Laser calibration lab record book #2 (2/2/95-3/21/97). Technical Report L0249, the National Radio Astronomy Observatory, 1999.

[141] David H. Parker. Survey field book #2 10/96-8/00. Technical Report L0631, the National Radio Astronomy Observatory, 2000.

[142] David H. Parker. Level field book #1. Technical Report L0719, the National Radio Astronomy Observatory, 2001.

[143] David H. Parker. Survey fiel book #2 9/13/01-8/1/03. Technical Report L0726, the National Radio Astronomy Observatory, 2003.

[144] David H. Parker. Survey field book #4 3/22/02-10/09/03. Technical Report L0728, the National Radio Astronomy Observatory, 2003.

[145] David H. Parker, Frederic R. Schwab, and John Shelton. Calibration and modeling of a dual-axis inclinometer. GBT Memo 227, the National Radio Astronomy Observatory, 2004.

[146] David H. Parker, Bill Radcliff, and John Shelton. Advances in hydrostatic leveling with the nph6, and suggestions for further enhancements. GBT Memo 228, the National Radio Astronomy Observatory, 2004.

[147] John Shelton. Plots of interferometer vs ranger. Technical Report L0736, the National Radio Astronomy Observatory.

[148] David H. Parker. Deflection of feed arm by elevator. Technical Report L0607, the National Radio Astronomy Observatory, 2000.

[149] David H. Parker. GBT properties that should be quantified–draft. Technical Report L0694, the National Radio Astronomy Observatory, 2002.

[150] Frederic R. Schwab. Geometry of the primary surface if the gbt. Technical Report 28, GBT Memo Series, 1990.

[151] John M. Payne. Pointing and surface control of GBT. Technical Report 36, GBT Memo Series, 1990.

[152] C. J. Brockway. Gbt fine pointing. Technical Report 38, GBT Memo Series, 1990.

[153] John M. Payne. Fine pointing for the gbt. Technical Report 42, GBT Memo Series, 1990.

[154] Frederic R. Schwab. Orientation of the retroreflectors on the gbt primary surface. Technical Report 64, GBT Memo Series, 1991.

[155] David Seaman. Corner cube mounting. Technical Report 65, GBT Memo Series, 1991.

[156] Ronald J. Maddalena, Roger D. Norrod, and Steven D. White. Planned holographic measurements with the Green Bank Telescope. Technical Report 68, GBT Memo Series, 1991.

[157] John M. Payne and Richard F. Parker, David H. and Bradley. A rangefinder with fast multiple range capability. Technical Report 73, GBT Memo Series, 1992.

[158] John M. Payne. Pointing the gbt. Technical Report 84, GBT Memo Series, 1992.

[159] Donald C. Well. The gbt precision pointing system. Technical Report 85, GBT Memo Series, 1992.

[160] Robert D. Hall. GBT phases. Technical Report 113, GBT Memo Series, 1994.

[161] David H. Parker. Gbt actuator/retroreflector/panel spreadsheet. Technical Report 114, GBT Memo Series, 1994.

[162] J. J. Condon. Gbt pointing equations. Technical Report 75, GBT Memo Series, 1992.

[163] J. R. Fisher and F. J. Lockman. Observer monitor and control requirements. Technical Report 81, GBT Memo Series, 1992.

[164] Mark H. Clark. Gbt m&c requirements analysis model. Technical Report 88, GBT Memo Series, 1992.

[165] Mark H. Clark and J. R. Fisher. Gbt monitor and control design rationale. Technical Report 89, GBT Memo Series, 1992.

[166] Larry R. D'Addario. Comments on gbt memo no. 89: "gbt monitor and control design rationale. Technical Report 90, GBT Memo Series, 1992.

[167] J. R. Fisher and Mark H. Clark. Reply to gbt memo 90. Technical Report 92, GBT Memo Series, 1992.

[168] D. E. Hogg. A summary of the minimum requirements for the control and operation of the gbt in the initial phase. Technical Report 94, GBT Memo Series, 1992.

[169] L. Macknik, D. E. Hogg, and J. R. Fisher. Division of concerns in the gbt pointing correction system. Technical Report 103, GBT Memo Series, 1993.

[170] Carl Heiles and Ronald J. Maddalena. The gbt oberserver interface.1. pointing the gbt: The astronomical pointing system (aps). ramifications for m&c and aips++. Technical Report 105, GBT Memo Series, 1993.

[171] Ramon E. Creager. Laser ranging system zy software reference manual. Technical Report 111, GBT Memo Series, 1994.

[172] F. J. Lockman. Requirements on use of the GBT active surface. Technical Report 120, GBT Memo Series, 1995.

[173] D. E. Hogg and J. R. Fisher. A revised description of the gbt pointing system. Technical Report 122, GBT Memo Series, 1995.

[174] Ramon E. Creager. A networked frame grabber. Technical Report 123, GBT Memo Series, 1995.

[175] John M. Payne. Gbt dynamic pointing meeting. Technical Report 127, GBT Memo Series, 1995.

[176] Donald C. Wells and L. King. Gbt best-fitting paraboloid [bfp] in c. Technical Report 131, GBT Memo Series, 1995.

[177] Dr. Sebastion von Hoerner. Fast pointing change and small oscillation. Technical Report 132, GBT Memo Series, 1995.

[178] John M. Payne and D. T. Emerson. Active damping for the gbt arm. Technical Report 133, GBT Memo Series, 1995.

[179] M. M. McKinnon. Low tracking rates in azimuth. Technical Report 139, GBT Memo Series, 1995.

[180] Roger D. Norrod. On possible locations for a gbt quadrant detector. Technical Report 143, GBT Memo Series, 1996.

[181] John M. Payne. Monitoring the gbt arm movement. Technical Report 144, GBT Memo Series, 1996.

[182] Ziegler, Nichols, and Rochester. Optimum settings for automatic controllers. Technical Report L0769, the National Radio Astronomy Observatory, 1942.

[183] Amy Petticrew. Running the camera program remotely with pcanywhere. Technical Report L0098, the National Radio Astronomy Observatory, 1996.

[184] Ray Creager. The GBT laser metrology computer control system. Technical Report L0652, the National Radio Astronomy Observatory, 199.

[185] Tim Weadon. Repeatability measurements with the GBT corner setting tool. Technical Report L0519, the National Radio Astronomy Observatory, 1999.

[186] David H. Parker. The Green Bank Telescope panel setting tool instrumentation. GBT Memo 145, the National Radio Astronomy Observatory, 1996.

[187] David H. Parker, John M. Payne, John W. Shelton, and Timothy Lee Weadon. Instrument for setting radio telescope surfaces. GBT Memo 206, the National Radio Astronomy Observatory, 2000.